NASA Technical Memorandum 84564

NASA-TM-84564 19830005228

FINITE-ELEMENT ANALYSIS OF INITIATION, STABLE CRACK GROWTH, AND INSTABILITY USING A CRACK-TIP-OPENING DISPLACEMENT CRITERION

J. C. Newman, Jr.

October 1982

NASA
National Aeronautics and
Space Administration

Langley Research Center
Hampton, Virginia 23665

FINITE-ELEMENT ANALYSIS OF INITIATION, STABLE CRACK GROWTH, AND INSTABILITY USING A CRACK-TIP-OPENING DISPLACEMENT CRITERION

J. C. Newman, Jr.
NASA Langley Research Center
Hampton, Virginia 23665

ABSTRACT

An elastic-plastic (incremental and small strain) finite-element analysis was used with a crack-growth criterion to study crack initiation, stable crack growth, and instability under monotonic loading to failure of metallic materials. The crack-growth criterion was a critical crack-tip-opening displacement (CTOD) at a specified distance from the crack tip, or equivalently, a critical crack-tip-opening angle (CTOA). Whenever the CTOD (or CTOA) equaled or exceeded a critical value, the crack was assumed to grow. Single values of critical CTOD were used in the analysis to model crack initiation, stable crack growth, and instability for 7075-T651 and 2024-T351 aluminum alloy compact specimens. Calculated and experimentally measured (from the literature) CTOD values at initiation agreed well for both aluminum alloys. These critical CTOD values from compact specimens were also used to predict failure loads on center-crack tension specimens and a specially-designed three-hole-crack tension specimen made of the two aluminum alloys and of 304 stainless steel. All specimens were 12.7 mm thick. Predicted failure loads for 7075-T651 aluminum alloy and 304 stainless steel specimens were generally within ±15 percent of experimental failure loads, whereas the predicted failure loads for 2024-T351 aluminum alloy specimens were generally within ±5 percent of the experimental loads. The technique presented here can be used as an engineering tool to predict crack initiation, stable crack growth, and instability for cracked structural components from laboratory specimens, such as the compact specimen.

INTRODUCTION

Experiments on metals have shown that, under monotonic loading to failure, a crack goes through three stages of behavior: (1) a period of no crack growth, (2) a period of stable crack growth, and (3) crack-growth instability under load-control (or stable crack growth with decreasing load under displacement-control). In the past decade, the phenomenon of stable crack growth has been studied extensively using elastic-plastic finite-element methods [1-8]. These studies were conducted, first, to develop efficient techniques to simulate crack extension and, second, to study various local and global fracture criteria. Some of these criteria were crack-tip stress or strain, crack-tip-opening displacement or angle, crack-tip force, energy release rates, J-integral, and the tearing modulus. Of these, the crack-tip-opening angle (CTOA), or displacement (CTOD) at a specified distance from the crack tip, was shown to be most suited for modeling stable crack growth and instability during the fracture process [3,7,8]. But some discrepancies among the various analyses have been observed at initiation of stable crack growth. de Koning [3] showed that CTOA was nearly constant from initiation, whereas Shih et al. [7] and Kanninen et al. [8] showed that CTOA at initiation was larger, and in some cases much larger, than the value needed for stable crack growth. On the other hand, Luxmoore et al. [9] have experimentally shown that CTOA (or CTOD) was constant from the onset of stable crack growth in two aluminum alloys, but have found different values for different crack configurations (center-crack and double-edge crack tension specimens). These results show the necessity for studying different crack configurations when assessing the validity of any fracture criteria.

One of the objectives of the present paper was to critically evaluate the CTOD growth criterion using an elastic-plastic finite-element analysis under monotonic loading to failure. In particular, the analysis was conducted to see whether or not the critical CTOD was constant during crack initiation, stable crack growth, and instability.

The second objective was to determine whether or not fracture data from laboratory specimens, such as the compact specimen, could be used to predict failure loads on other crack configurations. To assess the CTOD criterion, both experiments and analyses were conducted on several crack configurations made of various materials.

Fracture tests were conducted on three crack configurations: compact, center-crack tension, and a specially-designed three-hole-crack tension specimen (see Fig. 1) made of 7075-T651 aluminum alloy, 2024-T351 aluminum alloy, and 304 stainless steel. The compact specimens were tested by NASA Langley Research Center and Westinghouse Research and Development Laboratory [10] to provide basic fracture data (applied load against "physical" crack extension and failure loads.) Center-crack and three-hole-crack specimens were tested only by NASA Langley. The three-hole-crack specimen has a complicated stress-intensity factor solution, like that for a cracked stiffened panel.

In the finite-element analysis, a critical value of CTOD at a specified distance from the crack tip was chosen as the fracture criterion. During incremental loading to failure, whenever the CTOD equaled or exceeded a preset critical value (δ_c), the crack-tip node was released and the crack advanced to the next node. This process was repeated until crack growth became unstable at the failure load. Comparisons between experimental and calculated load against physical crack extension data were made on the compact specimens to determine the critical CTOD values. These critical CTOD values were then used to predict failure loads on other compact specimens, center-crack tension specimens and three-hole-crack tension specimens. Comparisons were made between predicted and experimental failure loads for all specimen types considered. Comparisons were also made between calculated and experimentally measured [11] CTOD values at initiation for the two aluminum alloys.

NOMENCLATURE

a	Crack length defined in Fig. 1, m
a_o	Initial crack length, m
$[B]$	Matrix relating total strains to nodal displacements, m^{-1}
$[D_e]$	Elasticity matrix relating stress to total strain, N/m^2
d	Minimum element size along crack line, m
$\{dP\}$	Incremental applied load vector, N
$\{dQ\}$	Incremental plastic load vector, N
dV_m	Differential volume of triangular element m, m^3
$\{d\varepsilon\}$	Incremental total strain vector
$\{d\sigma\}$	Incremental stress vector, N/m^2
$\{d\sigma_e\}$	Incremental elastic stress vector, N/m^2
$\{d\sigma^o\}$	Incremental "initial" stress vector, N/m^2
E	Young's modulus, N/m^2
G	Strain-energy-release rate, N/m
K	Stress-intensity factor, $N/m^{3/2}$
$[K_e]$	Elastic stiffness matrix, N/m
$[K_s]$	Diagonal matrix containing spring stiffnesses, N/m
k_{sx}, k_{sy}	Spring stiffness in x- and y-direction, respectively, N/m
M	Number of finite elements
N	Number of nodes
n	Ramberg-Osgood strain-hardening power
P	Applied load, N
P_f	Failure load, N
$\{P\}$	Applied load vector, N
$\{Q\}$	"Effective" plastic load vector, N
t	Specimen thickness, m

$\{U\}$	Generalized nodal displacement vector, m
W	Specimen width, m
Δa_p	Physical crack extension, m
δ_c	Critical crack-tip-opening displacement, m
δ_i	Crack-tip-opening displacement at initiation, m
ε	Uniaxial strain
κ	Ramberg-Osgood strain-hardening coefficient, N/m^2
σ	Uniaxial stress, N/m^2
σ_{ys}	Uniaxial yield stress (0.2 percent offset), N/m^2
σ_u	Uniaxial tensile strength, N/m^2

EXPERIMENTAL PROCEDURE

The experimental test program was conducted by NASA Langley Research Center and Westinghouse Research and Development Laboratory [10] as part of an ASTM E24 Round Robin on Fracture. Tests were conducted on compact specimens (with initial crack-length-to-width ratios, a_o/W, of 0.5) to obtain load against physical crack extension data and failure loads. The NASA Langley Research Center also conducted fracture tests on other compact specimens (with a_o/W equal to 0.3 and 0.7), center-crack tension specimens, and a "structurally-configured" specimen (with three circular holes and a crack emanating from one of the holes) subjected to tensile loading. The specimen configurations tested are shown in Figure 1. In addition, tensile specimens were tested to obtain uniaxial stress-strain curves.

Materials

The three materials tested were 7075-T651 aluminum alloy, 2024-T351 aluminum alloy, and 304 stainless steel. These materials were selected because they exhibit a wide range in fracture toughness behavior. They were obtained in plate form (1.2 m by 3.6 m) with a nominal thickness of 12.7 mm.

Specimen Configurations and Loadings

Four types of specimens were machined from one plate of each material. The specimens were: (1) Tensile, (2) Compact, (3) Center-crack tension, and (4) Three-hole-crack tension specimens. A summary of specimen types, nominal widths, and nominal crack-length-to-width ratios tested is shown in Table 1.

Tensile specimens.- Eight tensile specimens (ASTM E8) with square cross-section (12.7 by 12.7 mm) were machined from various locations in each plate of material. The specimens were machined to obtain tensile properties perpendicular to the rolling direction. Full engineering stress-strain curves were obtained from each specimen. The initial load rate was 45 kN/minute, but after yielding, the load rate

was set at 4.5 kN/minute. Average tensile properties (E, σ_{ys} and σ_u) are given in Table 2.

Compact specimens.- The compact specimen configuration is shown in Figure 1(a). The planar configuration is identical to the "standard" compact (ASTM E399) specimen, but the nominal thickness was 12.7 mm. Twenty-seven specimens were machined from each plate of material, and the cracks were oriented in the same direction (parallel to the rolling direction). The nominal widths, W, were 51, 102, and 203 mm, and the nominal crack-length-to-width ratios were 0.3, 0.5, and 0.7. All specimens were fatigue precracked according to the ASTM E399 requirements.

The specimens tested by Westinghouse ($a_o/W = 0.5$) were loaded under displacement-control conditions and periodically unloaded (about 15 percent at various load levels) to determine crack lengths from compliance [10,12]. But the specimens tested by NASA Langley were loaded under load-control conditions to failure. The initial load rates on the NASA Langley tests were about the same as those tested by Westinghouse. Load against crack extension data were obtained from visual observations and from unloading compliance data (at both the crack mouth and the load line). Initial crack lengths, a_o, and failure loads, P_f, were also recorded. The initial crack lengths were measured from broken specimens and were three-point weighted averages through the thickness ($3a_o = a_1 + 2a_2 + a_3$) where a_1 and a_3 were surface values and a_2 was the value in the middle of the specimen. Specimen dimensions, initial crack lengths and experimental failure loads are given in Tables 3-5 for the three materials. These experimental results will be presented and discussed later.

Center-crack and three-hole-crack tension specimens.- The center-crack and three-hole-crack specimen configurations are shown in Figures 1(b) and 1(c), respectively. Again, all specimens were machined so that the cracks were oriented parallel to the rolling direction. Four center-crack specimens (W = 127 and 254 mm) were machined from each plate of material. The nominal crack-length-to-width ratio

was 0.4. Eight three-hole-crack specimens (W = 254 mm) were also machined from each plate of material. The nominal crack lengths in the three-hole-crack specimen ranged from 13 to 102 mm. All center-crack and three-hole-crack specimens had 510 mm between griplines. The initial load rates were selected such that the initial stress-intensity factor rates were roughly the same (30 $MN/m^{3/2}$/minute) for all crack specimens. Again, initial crack lengths (three-point weighted average through the thickness) and failure loads were recorded. Specimen dimensions, initial crack lengths, and experimental failure loads are given in Tables 3-5 for the three materials. These results will be presented and discussed later.

FINITE-ELEMENT ANALYSIS OF FRACTURE

The elastic-plastic analysis of the three specimen types (Fig. 1) employed the finite-element method and the initial-stress concept [13,14]. The elastic-plastic analysis was based on incremental flow theory with a small strain assumption. The finite-element models for these specimens were composed of two-dimensional, constant strain, triangular elements under assumed plane-stress conditions. Several mesh patterns were used to model different size specimens so that the minimum element size, d, along the line of crack extension would be the same in all specimens. Fictitious springs were used to change boundary conditions associated with crack extension. The use of springs was found to be computationally efficient. For free nodes along the crack line, the spring stiffnesses were set equal to zero, and, for fixed nodes, the stiffnesses were assigned extremely large values. See Appendix A for details on the elastic-plastic finite-element analysis with crack extension.

Although the finite-element analysis (constant-strain elements) used here does not contain a singularity at the crack tip, such as the Hutchinson-Rice-Rosengren (HRR) singularity [15,16], the use of singularities may not be necessary. Singularities, which do not exist in real materials, are only mathematical consequences of continuum mechanics. The finite-element analysis with very small elements gives a high, but finite, strain concentration at the crack tip, like a crack in a real material.

The average material stress-strain curves used in the finite-element analysis were approximated by the Ramberg-Osgood equation [17] as

$$\varepsilon = \frac{\sigma}{E} + \left(\frac{\sigma}{\kappa}\right)^n \tag{1}$$

where K and n are the strain-hardening coefficient and power, respectively. Values of the constants are given in Table 2 for the three materials.

Crack-Growth Criterion

The crack-growth criterion used here was based on a critical crack-tip-opening displacement (δ_c) at a specified distance (d) from the crack tip. The distance d was the element size along the crack line, or in otherwords, d is the distance between the first free node and the crack tip. (The critical CTOD criterion is also equivalent to a critical CTOA criterion, since $CTOA = 2 \tan^{-1}(\delta_c/2d)$.) During incremental loading to failure, whenever the CTOD equaled or exceeded a preset critical value (δ_c), the crack-tip node was released (see Appendix A for details) and the crack advanced to the next node. This process was repeated until crack growth continued without any increase in load. The use of the CTOD (or CTOA) criterion does require that the absolute size (d) and arrangement of elements in the crack-tip region and along the line of crack extension be the same in all crack configurations considered.

The procedure used to establish the critical δ_c value and mesh size (d) is as follows. The mesh size in the crack-tip region of the large compact specimen (W = 203 mm) was systematically reduced until the calculated loads at initiation and at failure were reasonably close to the experimental values using a given value of δ_c. In other words, the mesh size was used as a variable to fit the experimental load against crack length data. After the mesh size d was determined, the final δ_c value was selected so that the mean of the calculated-to-experimental failure load ratio on the various size compact specimens (W = 51, 102, and 203 mm) with $a_o/W = 0.5$ was about unity. The critical δ_c value was then used to predict failure loads on other compact, center-crack tension, and three-hole-crack tension specimens.

The typical crack-growth behavior that was obtained from the finite-element analysis using the critical CTOD criterion is shown in Figure 2. Applied load is plotted against crack length. During initial loading, a plastic zone developed at and to the right of the crack tip as illustrated in Insert (a). At a certain load, the CTOD became critical (δ_c) and the crack moved forward one element size (d) while the applied load was held constant. The CTOD for the new crack tip was found to be less than the critical value. The dashed curve in Insert (b) shows what the crack-surface displacements would have been if residual plastic deformations had not been retained in the material to the left of the crack tip. The plastic deformations remaining in the wake of the advancing crack (lightly shaded region to the left of the crack tip) caused the new displacements to be substantially less than that for the crack without the "plastic wake". The corresponding crack-tip strains were also less for the crack with the plastic wake than for the crack without the plastic wake [5]. Thus, an increase in applied load was required to make the CTOD critical and to advance the crack further. This process was repeated until crack growth became unstable (continuous crack growth with no further increase in load). At the instability load, the CTOD value at the new crack tips were always equal to or greater than the δ_c value and the crack continued to grow from node to node. If the analysis had been conducted under displacement-control, instead of load-control, then a reduction in applied load would have been required to maintain a constant δ_c.

Compact Specimens

A typical finite-element model (Mesh A) for one-half of the compact specimen is shown in Figure 3. The crack line was a line of symmetry. The minimum element size along the crack line was 0.00625 W_o for this mesh pattern. W_o is overall width of

compact specimen. (The large number of elements around the pin-loaded hole was not necessary for this study. This particular mesh was used in a previous analysis to study the deformations around the hole and was used here only for convenience.)

Critical CTOD.- A comparison between experimental and calculated load against physical crack extension data on a 7075-T651 aluminum alloy compact specimen is shown in Figure 4. The symbols show the average experimental crack extension measurements made using visual and unloading compliance (load-line and crack mouth) methods [10]. The solid lines show calculations made using three different mesh sizes (Mesh A, B and C) in the crack-tip region. The critical CTOD values (δ_c) for each mesh size was selected (by trial and error) to give about the same failure load as measured on the compact specimen. The δ_c values, shown on the figure, were lower for smaller mesh sizes. Smaller mesh sizes also gave lower loads at initiation of crack growth. The calculated crack-growth behavior from Mesh C (d = 0.4 mm) agreed well with the experimental data, up to maximum load.

The final δ_c value for the 7075-T651 aluminum alloy was selected so that the mean of the calculated-to-experimental failure load ratio on the various size compact specimens with $a_o/W = 0.5$ was about unity. Mesh C was used for the 203 mm-wide specimen; Mesh B and A with all coordinates scaled by a factor of 0.5 and 0.25, respectively, were used for the 102 and 51 mm-wide specimens, so that the element size along the crack line was 0.4 mm in all meshes. A comparison between experimental and calculated load against crack extension data on two compact specimen sizes (W = 51 and 203 mm) is shown in Figure 5. The large solid symbols show the experimental data from a single test and the respective bars indicate the range and mean of failure (or maximum) load on four or five tests. The bars are placed at the average value of crack extension at maximum load. The solid lines show the calculated crack-growth behavior from the finite-element analysis with $\delta_c = 0.0216$ mm and $d = 0.4$ mm for both specimens. The tests were conducted under displacement-control conditions, whereas the analysis was conducted under load-control conditions. Thus, calculations were not made beyond maximum load. The calculated failure load on the large specimen was about 5 percent lower than the average experimental failure load. But for the small specimen, the calculated failure load was about 10 percent higher than the

average experimental failure load. The calculated failure loads for all compact specimens with a_o/W equal to 0.5 are given in Table 3. The mean of the ratios of calculated-to-experimental failure load was about 1.01.

For convenience, the same mesh size (d = 0.4 mm) used for the 7075-T651 aluminum alloy specimens was also used for the 2024-T351 aluminum alloy and 304 stainless steel specimens.

A comparison between experimental and calculated load against physical crack extension data 2024-T351 aluminum alloy compact specimens is shown in Figure 6. Again, the symbols show average experimental crack extension measurements made on two compact specimens using visual and unloading compliance data [10]. The respective bars indicate the range and mean of failure loads on four or five tests. A critical CTOD value was selected so that the mean of the calculated-to-experimental failure load ratio on the various size compact specimens with $a_o/W = 0.5$ was about unity. Again, the solid lines show the calculated crack-growth behavior from the finite-element analysis with $\delta_c = 0.0457$ mm and $d = 0.4$ mm. The calculated behavior at initiation and at instability (maximum load) agreed well with the experimental data. Some discrepancies between calculated and experimental behavior was observed for the stable crack growth region. However, the calculated failure loads on the large and small compact specimens were within 5 percent of the average experimental failure loads.

As with the other materials, the critical CTOD value for 304 stainless steel specimens was selected so that the mean of the calculated-to-experimental failure load ratio on the various size compact specimens (W = 51, 102, and 203 mm) with $a_o/W = 0.5$ was, again, about unity. The critical CTOD value (δ_c) was 0.356 mm with $d = 0.4$mm. The 304 stainless steel compact specimens exhibited large deformations and rotations. Because the finite-element analysis was based on a small strain assumption, no comparisons were made between calculated and experimental crack growth.

Comparison of Calculated and Experimental CTOD Values.- Paleebut [11] used a laser-interferometric displacement technique to measure crack-opening displacements near the tip of a crack in 7075-T651 and 2024-T351 aluminum alloy compact specimens (W = 51 mm). The specimen thicknesses ranged from 3 to 25 mm. Only the results for 13 mm-thick specimens were of interest here. The specimens were fatigue precracked according to ASTM E399 requirements to a specified crack length ($a_o/W = 0.5$) and then two indentations 0.1 mm apart were placed across the fatigue crack about 0.1 mm from the crack tip. The specimens were then statically pulled to failure and load against CTOD traces were obtained from the test. The first indication of a major "pop-in" was taken to be the CTOD at initiation (δ_i). These experimental values are given in the following table:

		Experimental	Calculated
Material	t, mm	δ_i, mm	δ_c, mm
7075-T651	13	0.021	0.0216
2024-T351	13	0.048	0.0457

The critical CTOD values (δ_c) determined from fitting the finite-element analysis to load against crack extension data for the two materials are also shown for comparison. Despite the fact that the δ_c values in the analyses were measured at 0.4 mm from the crack tip, instead of 0.1 mm, as in the experiments, the agreement is extremely good. This good agreement may be due to crack tunneling. Cracks in 13-mm thick compact specimens tend to tunnel in the interior. Consequently, the "effective" distance from the crack tip to the measurement point would have been larger than 0.1 mm. For the 7075-T651 material, the average tunneling was about 0.6 mm, whereas for the 2024-T351 material the average tunneling was about 1 mm. The 0.4 mm used in the analysis was less than the average tunneling for both materials.

Failure Load Predictions.- Having determined the critical CTOD values for the three materials, the finite-element analysis was used to predict failure loads on compact specimens with $a_o/W = 0.3$ and 0.7. Figures 7, 8, and 9 show experimental (symbols) and predicted failure loads plotted against a_o/W for 7075-T651 aluminum alloy, 2024-T351 aluminum alloy, and 304 stainless steel, respectively. The predicted failure loads were calculated for $a_o/W = 0.3$, 0.5, and 0.7; and a curve was drawn through the results. A failure load prediction was not made on the large 304 stainless steel specimen with $a_o/W = 0.3$ because of the excessive computer cost. All predictions were within ±10 percent of the experimental failure loads, except for some results on the 304 stainless steel specimens. The predicted results on the steel specimens showed some systematic errors in failure load predictions with a_o/W and W, but all predicted failure loads were within ±15 percent of experimental loads. The larger and systematic errors on the steel specimens were probably due to using a small strain analysis for a large deformation problem.

Experimental and predicted failure loads for compact specimens are given in Tables 3-5 for the three materials.

Center-Crack Tension Specimens

Because the critical CTOD values were determined from compact specimens, the good failure load predictions on other compact specimens may have been fortuitous. To test the CTOD criterion and to determine whether or not fracture data from compact specimens could be used to predict failure of other crack configurations, center-crack tension specimens were also tested and analyzed.

Figure 10 shows the finite-element meshes used to model the two center-crack tension specimens (W = 127 and 254 mm). Because of symmetry, only one-quarter of the specimen was modelled. Insert A, along the crack line, shows the typical element sizes and patterns in the crack-tip region for the two specimen sizes. The minimum element size along the crack line for both specimens was 0.4 mm.

The finite-element analysis with the CTOD criterion was used to predict failure loads on the center-crack tension specimens made of the three materials (see Tables 3-5). Figure 11 shows experimental (symbols) and predicted failure loads plotted against specimen width for a nominal $a_o/W = 0.4$. The predicted failure loads were made at $W = 127$ and 254 mm, and a line was drawn through the results. All predictions were within about ±10 percent of experimental failure loads for all materials.

Three-Hole-Crack Tension Specimens

To verify the general applicability of the CTOD criterion to complex cracked components, a structurally-configured specimen, the three-hole-crack tension specimen (Fig. 1(c)) was also tested and analyzed. The three-hole-crack specimen was designed to give a complicated stress-intensity factor solution, like that for a cracked stiffened panel. Although the stress-intensity factor solution was not used in the fracture analysis, the stress-intensity factor solution will be used in the discussion of results. In the following, the stress-intensity factor solution and failure load predictions on the three materials are presented.

Stress-Intensity Factor Solution.- The stress-intensity factor solution for the three-hole-crack tension specimen was obtained by using a two-dimensional elastic finite-element analysis [14]. The finite-element mesh for one-half of the specimen is shown in Figure 12. The minimum element size was 0.00625W. Stress-intensity factors as a function of crack length were obtained by using a local-energy approach proposed by Irwin [18]. To verify the local-energy approach and mesh pattern in the crack-tip region, compact and center-crack tension specimens were also analyzed. The details of the approach are given in Appendix B.

The stress-intensity factor solution for the three-hole-crack tension specimen (Fig. 1(c)) is shown in Figure 13. The symbols show the finite-element results. Stress-intensity factors were normalized by gross applied stress (P/Wt) and are

plotted against crack-length-to-width ratio (a/W) with W = 254 mm. Crack length is measured from the edge of the small hole. The dash-dot line shows the centerline of the two large holes. This solution simulates the solution for a cracked stiffened panel [19], when the centerline of the stiffener is located at a/W = 0.25 (dash-dot line). The stress-intensity factors have a minimum value near the centerline of the two large holes, or a stiffener, in the case of a stiffened panel.

Failure Load Predictions.- During the failure of the three-hole-crack specimens with a_o/W less than 0.3, large amounts of stable crack growth were expected (as much as 65 mm for $a_o/W = 0.05$) because of the stress-intensity factor solution shown in Figure 13. During monotonic loading, as the crack stably tears toward the centerline of the large holes, the stress-intensity factor decreases. An increase in load is required to cause further stable crack growth. Crack-growth instability should only occur when the crack has passed the minimum stress-intensity factor at an a/W value of about 0.3. The same general behavior might intuitively be expected for elastic-plastic materials. The fracture tests on the three materials and the finite-element analysis will test this hypothesis.

To save computer time and cost, the small elements (d = 0.4 mm) were used only between a/W values of 0.275 and 0.375, for $a_o/W \leq 0.25$ because the crack should stably tear to an a/W value of about 0.3. At this point, the crack will be located in the small element region. For $a_o/W = 0.3$, 0.35, and 0.4, the small element pattern was placed at the appropriate location along the crackline so that all stable crack growth would occur in the small element region. But for a_o/W less than 0.275 ($a_o < 70$ mm) stable crack growth would occur in a region with larger element sizes than 0.4 mm. To use the larger element sizes, the CTOD criterion was modified as follows. The large compact specimen (W = 203 mm) with $a_o/W = 0.5$ was reanalyzed with three different element sizes along the line of crack extension. Critical CTOD values needed to predict only the experimental failure loads on the three materials were determined. These results are shown in Figure 14. The critical

CTOD (δ_c') for a given element size (d′) normalized by the critical CTOD (δ_c) for an element size (d) of 0.4 mm is plotted against the element size ratio (d′/d). Symbols show the finite-element results for the three materials. The solid line is an equation fit to the results. The equation

$$\delta_c' = \delta_c\left[1 + \frac{2}{3}\left(\frac{d'}{d} - 1\right)\right] \tag{2}$$

was used to determine the δ_c' value for any value of element size d′. δ_c and d are shown on Figure 14 for the three materials. (The dashed line indicates the relationship between δ_c' and d′ needed for a constant CTOA.)

Motion pictures (200 frames per second) were taken of some of the three-hole crack specimen tests. A volt meter was used to indicate applied load in the movie. Load against crack length measurements taken from these motion pictures are shown in Figure 15. The initial crack lengths, a_o, were about 25.4 mm. The symbols show experimental data on 7075-T651 and 2024-T351 aluminum alloy specimens and the solid lines show the prediction from the finite-element analysis. The solid symbols show the final crack lengths near maximum load conditions. As expected, the final crack lengths were pass the centerline of the large holes and were very near the minimum stress-intensity factor location in Figure 13. Predictions on the 7075-T651 aluminum alloy specimen were in fair agreement with the experimental results. The predicted failure load was about 16 percent lower than the experimental failure load. Whereas, predictions on the 2024-T351 aluminum alloy specimen agreed well with the experimental results. Here the predicted failure load was only 6 percent higher than the experimental failure load. However, the predicted crack lengths at instability (crack length at first attainment of maximum load) were less than the experimental values, especially on the 2024-T351 specimen. This may have been caused by the size of the load step used in the analysis since the predicted

curve is nearly horizontal near maximum load. Photographs from motion picture frames near maximum (failure) load condtions are shown in Figure 16 for the three materials. Figure 16(c) illustrates why finite-deformation analyses may be necessary to improve the predictions for the 304 stainless steel specimens.

A comparison between predicted and experimental failure load for various initial crack lengths for the three materials is shown in Figure 17. Again, symbols show the experimental failure loads and the solid curves show the predicted results from the finite-element analysis. Predictions were not made on most of the 304 stainless steel specimens because of the high computer cost. The predicted failure loads on 7075-T651 aluminum alloy specimens were 2 to 18 percent lower than the experimental failure loads. The largest errors occurred at the smallest crack lengths. This was probably caused by using the larger element sizes for a_o less than 70 mm. However, predicted failure loads on the 2024-T351 aluminum alloy specimens agreed well (1 to 6 percent) with the experimental loads. The predicted failure loads for the 304 stainless steel specimens were about 10 percent higher than the experimental results.

CONCLUSIONS

An elastic-plastic (incremental and small strain) finite-element analysis, in conjunction with a crack-growth criterion based on crack-tip-opening displacement, was used to study crack-growth behavior under monotonic loading to failure for three crack configurations and for three materials. Fracture tests were conducted on compact, center-crack tension, and a specially-designed three-hole-crack tension specimen made of 7075-T651 aluminum alloy, 2024-T351 aluminum alloy, and 304 stainless steel. In the analysis, the crack-growth criterion was a critical crack-tip-opening displacement (CTOD) at a specified distance from the crack tip. Whenever the CTOD equaled or exceeded a critical value (δ_c), the crack was assumed to grow. Comparisons were made with experimental data. This investigation supports the following conclusions:

(1) The present elastic-plastic analysis predicted three stages of crack-growth behavior, characteristic of metals, under monotonic loading to failure: (a) a period of no crack growth, (b) a period of stable crack growth, and (c) crack-growth instability under load-control conditions.

(2) Single values of critical CTOD (δ_c) used in the present analysis were found to reasonably model crack initiation, stable crack growth, and instability for 7075-T651 and 2024-T351 aluminum alloy compact specimens.

(3) Calculated CTOD values agreed well with experimentally measured (from the literature) values for crack-growth initiation for the two aluminum alloys.

(4) Critical CTOD (δ_c) values from compact specimens were used in the present analysis to predict failure loads on center-crack tension and three-hole-crack tension specimens generally within ±15 percent of experimental failure loads on 7075-T651 aluminum alloy and 304 stainless steel specimens, and within ±6 percent of experimental failure loads on 2024-T351 aluminum alloy specimens.

APPENDIX A.- ELASTIC-PLASTIC FINITE-ELEMENT ANALYSIS WITH CRACK EXTENSION

The elastic-plastic analysis of the compact, center-crack tension, and three-hole-crack specimens employed the finite-element method and the initial-stress concept as described in References 13 and 14. The finite-element models were composed of two-dimensional constant-strain triangular elements. In the initial-stress approach, the load-displacement relations for a discretized structure are written to include the effects of "initial" stresses, which are required in order to satisfy the yield criterion (von Mises) for an elastic-plastic material. These initial stresses produce effective plastic-load vectors which are applied to all elements which have become plastic and which maintain the permanent plastic deformation on those elements while the external loads are applied. The governing matrix equations for a discretized structure are reviewed only briefly here to demonstrate how the material nonlinearity is accounted for and what is required to treat crack extension.

Solution Procedure for Elastic-Plastic Structures

The application of the finite-element method to problems involving linearly elastic materials is straightforward because the material properties are constant and only one solution is required to obtain displacements for the elastic structure. However, for elastic-plastic structures the coefficients in the stiffness matrix are functions of loading. Thus, the displacements are usually obtained by applying small load increments to the structure and either updating the coefficients of the stiffness matrix or applying an "effective" plastic-load vector after each load increment.

In general, the matrix equation which governs the response of a discretized structure under loads which cause plastic deformation is

$$[K_e]\ \{U\}_I^i = \{P\}^i + \{Q\}_{I-1}^{i-1} \tag{3}$$

where $[K_e]$ is the elastic stiffness matrix, $\{U\}$ is the generalized nodal displacement vector, $\{P\}$ is the applied load vector, and $\{Q\}$ is the "effective" plastic-load vector which accounts for elements in a plastic state. In the initial-stress method, the solution to an elastic-plastic problem is obtained by applying a series of small load increments to the structure until the desired load is reached ($\{P\}^i = \{P\}^{i-1} + \{dP\}$). The load increment was chosen as 10 percent of the applied load required to yield the highest stressed element at the crack tip. The superscript i in Equation (3) denotes the current load increment and $i - 1$ denotes the preceding increment. After each load increment an iterative process is required to stabilize the plastic-load vector. The superscript I in Equation (3) denotes the current iteration and $I - 1$ denotes the preceding iteration. During the i^{th} increment a purely elastic problem is solved and the increments in total strain $\{d\varepsilon\}$ and corresponding elastic stress $\{d\sigma_e\}$ are computed from the displacements for every element. Because of the material nonlinearity the stress increments are not, in general, correct. If the correct stress increment for the corresponding strain increment is $\{d\sigma\}$, then a set of body forces or plastic-load vectors $\{dQ\}$ caused by the "initial" stress $\{d\sigma^o\}$ ($= \{d\sigma_e\} - \{d\sigma\}$) is required to maintain the stress components on the yield surface. The correct stress increment $\{d\sigma\}$ is computed from the equations given in Reference 13. The plastic load increments are computed from

$$\{dQ\} = \sum_{m=1}^{M} \int [B]^T \{d\sigma^o\} \, dV_m \tag{4}$$

where M is the total number of elements, $[B]$ is the strain-displacement relationship, and the superscript T denotes the matrix transpose. The integration is taken over the volume of each element and the summation is over all elements in the structure. For elements which are in an elastic state, $\{d\sigma^o\} = 0$. The total plastic-load

vector is then computed as

$$\{Q\}_I^i = \{Q\}_{I-1}^{i-1} + \{dQ\} \tag{5}$$

At the second stage of computation the new force system $\{Q\}_I^i$ is added to the applied load vector and a new set of displacements is obtained. Again, some of the stresses are likely to exceed the yield criterion and a new set of plastic-load increments is computed. The iteration process is repeated until the effective stress (octahedral shear stress) [20] was within 2 percent of the current flow stress of the material. Usually, 5 to 15 iterations are required to stabilize the plastic-load vector. However, for configurations which have large strain gradients, more iterations are required. For the cracked specimens considered here and the particular element meshes used, 5 to 100 iterations were required. For the 304 stainless steel specimens, as many as 400 iterations were required in some cases.

Solution Procedure for Changing Boundary Conditions

The finite-element analysis of an extending crack under monotonic loading must be able to account for changing boundary conditions. Usually, boundary conditions (free or fixed) in the finite-element method are satisfied by adding equations to, or deleting equations from, the overall system of equations. But the approach selected here was to connect two springs to each boundary node. One spring was used to satisfy boundary conditions in the x-direction, and the other to satisfy conditions in the y-direction. Therefore, all nodes in the system had two degrees of freedom. For free nodes, the spring stiffness, k_{sx} or k_{sy}, was set equal to zero. For fixed nodes, the spring stiffness was assigned an extremely large value (10^7 times the modulus of elasticity of the plate material). The spring stiffness was added to the diagonal coefficient in the conventional elastic stiffness matrix.

The use of springs to satisfy boundary conditions was selected because an efficient technique to modify coefficients of the elastic stiffness matrix was incorporated into the nonlinear analysis program. This technique involved modifying the coefficients of the Cholesky decomposition [21] of the elastic stiffness matrix. A detailed discussion of the coefficient-modification technique may be found in References 14 or 21.

The coefficients of the elastic stiffness matrix are obtained from

$$[K_e] = \sum_{m=1}^{M} \int [B]^T [D_e][B] \, dV_m + [K_s] \tag{6}$$

where $[D_e]$ is the elasticity matrix and the diagonal matrix $[K_s]$ contains the elastic stiffness of the springs connected to the boundary nodes.

The procedure for treating the nonlinear material behavior in the presence of changing boundary conditions remains unchanged from that previously presented for an elastic-plastic structure, except that the nodal displacement for the node closest to the crack tip was monitored to determine whether the crack-tip node was to be released (crack extends).

To extend the crack, the stiffness of the spring at the crack-tip node was set equal to zero ($[K_e]$ modified) and the nodal force that was carried by the spring was then applied to the crack-tip node. The crack-tip force was arbitrarily chosen to be released in three equal load steps. Previous studies had indicated that the number of load steps (1, 10, and 50) had little effect on the final displacements for the small element sizes used here. When the nodal force went to zero, the crack tip had advanced to the next node. To insure that the stresses and total strain increments in the adjacent elements satisfied the yield condition and the Prandtl-Reuss flow rule [20], the iterative procedure, previously discussed, was

used to redistribute the force previously carried by the broken node, and to stabilize the plastic-load vector.

APPENDIX B.- STRESS-INTENSITY FACTORS FROM FINITE-ELEMENT ANALYSIS

The stress-intensity factor solution for the three-hole-crack tension specimen (Fig. 1(c)) was obtained by using a two-dimensional elastic finite-element analysis [14] under plane-stress conditions. The stress-intensity factors were obtained by using a local-energy approach [18]. To verify the finite-element approximation of the local-energy approach and the mesh pattern in the crack-tip region, compact and center-crack tension specimens were also analyzed.

The finite-element meshes used for the compact, center-crack, and three-hole-crack specimens are shown in Figures 3, 10(a), and 12, respectively. The element-mesh pattern along the crack line and in the crack-tip region were the same in all meshes. The smallest element size along the crack line was 0.00625 times the overall specimen width. The number of elements (constant strain) and number of nodes are shown on the figures.

The strain-energy-release rate, G, is obtained from Reference 18 as

$$G = \lim_{\Delta a \to 0} \frac{1}{\Delta a} \int_0^{\Delta a} \sigma_{yy} \, V \, dx \tag{7}$$

where Δa is a small amount of crack extension, σ_{yy} is the normal stress along the crack line, and V is the crack-surface displacement.

The strain-energy release rate was obtained from the elastic finite-element analysis by using nodal forces and displacements. The value of G was computed at two different values of crack extension (Δa and $2\Delta a$) and the value at $\Delta a = 0$ was obtained by linear extrapolation. At a given crack length a, the node at the crack tip is defined as node 1; the node at $a + \Delta a$ is defined as node 2; and the node at $a + 2\Delta a$ is defined as node 3. With unit load applied to the crack configuration of interest, the nodal forces at node 1 and 2 are computed. The crack is then allowed

to extend (elastically) from node 1 to node 2. The displacement at node 1 is now computed. The previous force at node 1, F_1, is the force required to close the crack surface over the length Δa. The first estimation for G is computed as

$$G_1 = \frac{F_1 V_1}{t\Delta a} \tag{8}$$

Next, the crack is allowed to extend from node 2 to node 3. The total amount of crack extension from crack length a is $2\Delta a$. The displacements at nodes 1 and 2 are now computed and used to obtain the second estimate for G as

$$G_2 = \frac{F_1 V_1 + F_2 V_2}{t2\Delta a} \tag{9}$$

The value of G at $\Delta a = 0$ was obtained by linear extrapolation and is given by

$$G = 2G_1 - G_2 \tag{10}$$

The stress-intensity factor K was obtained from the plane-stress relation between K and G as

$$K = \sqrt{GE} \tag{11}$$

Compact Specimen

The stress-intensity factors for the compact specimen (Figure 1(a)) were calculated for crack-length-to-width ratios, a/W, ranging from 0.2 to 0.8.

The finite-element results were compared with the results from the equation

$$K = \frac{P}{t\sqrt{W}} \frac{(2 + \lambda)}{(1 - \lambda)^{3/2}} (0.886 + 4.642 - 13.32\lambda^2 + 14.72\lambda^3 - 5.6\lambda^4) \qquad (12)$$

where $\lambda = a/W$ [22]. The finite-element results were 1 to 3.4 percent lower than the results from the equation. The largest errors occurred at the largest values of a/W.

Center-Crack Tension Specimen

The stress-intensity factors for the center-crack tension specimen (Figure 1(b)) were calculated for crack-length-to-width ratios, 2a/W, ranging from 0.2 to 0.9. Again, the finite-element results were compared with the well-known equation from Reference 23

$$K = \frac{P}{Wt} \sqrt{\pi a \sec\left(\frac{\pi a}{W}\right)} \qquad (13)$$

The finite-element results were 1.4 to 3.1 percent lower than the results from the equation. Again, the largest errors occurred at the largest values of 2a/W.

Three-Hole-Crack Tension Specimen

The stress-intensity factors for the three-hole-crack specimen (Fig. 1(c)) is shown in Figure 13. On the basis of the results obtained on the compact and center-crack specimens, the finite-element results are expected to be 1 to 3 percent lower than the "true" stress-intensity factor solution.

REFERENCES

[1] Anderson, H., "A Finite-Element Representation of Stable Crack Growth," J. Mech. Phys. Solids, Vol. 21, 1973, pp. 337-356.

[2] Kobayashi, A. S.; Chiu, S. T.; and Beeuwkes, R., "A Numerical and Experimental Investigation on the Use of the J-Integral," Engineering Fracture Mechanics, Vol. 5, No. 2, 1973, pp. 293-305.

[3] de Koning, A. U., "A Contribution to the Analysis of Slow Stable Crack Growth," The Netherlands, National Aerospace Laboratory Report NLR MP 75035U, 1975.

[4] Light, M. F.; Luxmoore, A.; and Evans, W. T., "Prediction of Slow Crack Growth by a Finite Element Method," Int. J. of Fracture, Vol. 11, 1975, pp. 1045-1046.

[5] Newman, J. C., Jr., "Finite-Element Analysis of Crack Growth Under Monotonic and Cyclic Loading", ASTM STP 637, American Society for Testing and Materials, 1977, pp. 56-80.

[6] Rousselier, G., "A Numerical Approach for Stable-Crack-Growth and Fracture Criteria," Proceedings of the Fourth International Conference on Fracture, Vol. 3, 1977.

[7] Shih, C. F.; de Lorenzi, H. G.; and Andrews, W. R., "Studies on Crack Initiation and Stable Crack Growth," ASTM STP 668, American Society for Testing and Materials, 1979, pp. 65-120.

[8] Kanninen, M. F.; Rybicki, E. F.; Stonesifer, R. B.; Broek, D.; Rosenfield, A. R.; and Halin, G. T., "Elastic-Plastic Fracture Mechanics for Two-Dimensional Stable Crack Growth and Instability Problems," ASTM STP 668, Amer. Soc. for Testing and Materials, 1979, pp. 121-150.

[9] Luxmoore, A.; Light, M. F.; and Evans, W. T., "A Comparison of Energy Release Rates, the J-Integral and Crack Tip Displacements," Int. J. of Fracture, Vol. 13, 1977, pp. 257-259.

[10] McCabe, D. E., "Data Development for ASTM E24.06.02 Round Robin Program on Instability Prediction", NASA CR-159103, August 1979.

[11] Paleebut, S., "CTOD and COD Measurements on Compact Tension Specimens of Different Thicknesses," M.S. Thesis, Michigan State University, 1978.

[12] Clarke, G. A.; Andrews, W. R.; Paris, P. C.; and Schmidt, D. W., "Single Specimen Tests for J_{IC} Determination", Mechanics of Crack Growth, ASTM STP 590, American Society for Testing and Materials, 1976, pp. 27-42.

[13] Zienkiewicz, O. C.; Valliappan, S.; and King, I. P., "Elasto-Plastic Solutions of Engineering Problems, Initial Stress, Finite Element Approach," International J. for Numerical Methods in Engineering, Vol. 1, 1969, pp. 75-100.

[14] Newman, J. C., Jr., "Finite-Element Analysis of Fatigue Crack Propagation - Including the Effects of Crack Closure," Ph.D. Thesis, Virginia Polytechnic Institute and State University, May 1974.

[15] Hutchinson, J. W., "Singular Behavior at End of Tensile Crack in Hardening Material," J. Mech. Phys. Solids, Vol. 16, 1968, pp. 13-31.

[16] Rice, J. R. and Rosengren, G. F., "Plane Strain Deformation Near Crack Tip in Power-Law Hardening Material," J. Mech. Phys. Solids, Vol. 16, 1968, pp. 1-12.

[17] Ramberg, W. and Osgood, W. R., "Description of Stress-Strain Curves by Three Parameters," NACA TN-902, 1943.

[18] Irwin, G. R., "Analysis of Stresses and Strains Near the End of a Crack Traversing a Plate," Transactions, ASME, J. of Applied Mechanics, 1957.

[19] Poe, C. C., Jr., "Stress Intensity Factor for a Cracked Sheet with Rivited and Uniformly Spaced Stringers," NASA TR-358, May 1971.

[20] Mendelson, A., Plasticity: Theory and Application, The MacMillan Co., New York, 1968.

[21] Gill, P. E.; Golub, G. H.; Murray, W.; and Saunders, M. A., "Methods for Modifying Matrix Factorizations," Computer Science Department, Stanford University, STAN-CS-72-322, pp. 18-24, 1972.

[22] Srawley, J. E., "Wide Range Stress-Intensity Factor Expressions for ASTM E399 Standard Fracture Toughness Specimens," Int. J. of Fracture, Vol. 12, June 1976, p. 475.

[23] Brown, W. F., Jr. and Srawley, J. E., Plane Strain Crack Toughness Testing of High Strength Metallic Materials, ASTM STP-410, American Society for Testing and Materials, 1969, p. 77-79.

Table 1--Test specimen matrix and number of specimens for 7075-T651, 2024-T351, and 304 stainless steel.

Specimen Type	Nominal Width, mm	Nominal Crack-Length-to-Width Ratio			
		0.3	0.4	0.5	0.7
Compact	51	2	...	5[a]	2
Compact	102	2	...	5[a]	2
Compact	203	2	...	5[a]	2
Center-Crack	127	...	2	...	...
Center-Crack	254	...	2	...	...
Three-Hole Crack	254	8 ($0.05 \leq a_o/W \leq 0.4$)			
Tensile[a]	12.7	...			

[a]Data used to determine δ_c.

Table 2--Average tensile properties of the three materials.[a]

Material	E, MN/m^2	σ_{ys}, MN/m^2	σ_u, MN/m^2	κ, MN/m^2	n
7075-T651	71,700	530	585	640	30
2024-T351	71,400	315	460	550	10
304 Stainless Steel	203,000	265	630	745	5

[a]Average values from eight tests.

Table 3--Aluminum alloy 7075-T651.

(a) Compact specimens.

t, mm	W, mm	a_o, mm	Experimental P_f, kN	$\frac{P_{pred}}{P_{exp}}$
12.4	51	16.1	16.1	1.00
12.5	51	15.4	16.0	1.01
12.7[a]	51	25.6	8.73	1.10
12.8[a]	51	25.6	8.85	1.08
12.6	51	25.4	8.54	1.12
12.6	51	25.9	8.85	1.08
12.6	51	35.4	3.75	1.03
12.5	51	36.3	3.34	1.15
12.7	102	31.8	27.4	0.95
12.7	102	30.6	27.2	0.95
12.8[a]	102	50.8	15.5	0.95
12.7[a]	102	50.7	15.5	0.95
12.8[a]	102	51.4	14.5	1.02
12.7	102	50.9	15.1	0.98
12.8	102	51.4	15.1	0.98
12.6	102	71.2	5.78	1.08
12.7	102	71.0	5.65	1.11
12.7	203	60.6	47.4	0.90
12.8	203	60.4	46.3	0.92
12.8[a]	203	102.0	24.1	1.00
12.7[a]	203	102.2	24.1	1.00
12.8[a]	203	100.8	25.4	0.95
12.8	203	101.2	25.7	0.94
12.8	203	101.2	26.2	0.92
12.8	203	142.0	10.2	0.97
12.7	203	142.2	10.5	0.95

[a]Tested at Westinghouse Research Laboratory [10].

Table 3--(Continued).

(b) Center-crack tension specimens.

t, mm	W, mm	a_o, mm	Experimental P_f, kN	$\frac{P_{pred}}{P_{exp}}$
12.8	127	26.4	209	0.97
12.8	127	24.9	200	1.02
12.8	254	49.8	365	0.89
12.7	254	49.1	356	0.91

(c) Three-hole crack specimens.

t, mm	W, mm	a_o, mm	Experimental P_f, kN	$\frac{P_{pred}}{P_{exp}}$
12.8	254	11.9	696	0.83
12.8	254	25.5	685	0.84
12.7	254	39.7	698	0.82
12.7	254	50.5	651	0.88
12.8	254	64.8	620	0.92
12.7	254	75.6	578	0.98
12.8	254	90.1	462	0.96
12.8	254	100.8	362	0.95

Table 4--Aluminum Alloy 2024-T351.

(a) Compact specimens.

t, mm	W, mm	a_o, mm	Experimental P_f, kN	$\frac{P_{pred}}{P_{exp}}$
12.4	51	16.1	29.8	0.98
12.3	51	16.0	29.5	0.99
12.6[a]	51	26.5	14.2	1.01
12.5[a]	51	26.3	14.7	0.97
12.5[a]	51	26.1	14.8	0.97
12.3	51	26.1	14.5	0.98
12.4	51	26.4	14.7	0.97
12.3	51	36.2	5.22	0.95
12.3	51	36.3	5.29	0.93
12.5	102	31.4	54.7	1.06
12.5	102	31.2	54.7	1.06
12.5[a]	102	51.9	28.8	0.98
12.6[a]	102	51.6	28.9	0.98
12.6[a]	102	51.4	29.8	0.95
12.5	102	51.6	28.2	1.00
12.5	102	51.9	28.7	0.99
12.6	102	71.2	10.1	0.99
12.5	102	71.4	10.1	0.98
12.5	203	61.8	98.5	0.93
12.6	203	61.7	100.3	0.92
12.6[a]	203	102.4	52.1	1.04
12.6[a]	203	102.5	51.9	1.04
12.5	203	102.2	52.3	1.04
12.6	203	102.2	52.0	1.04
12.5	203	142.9	18.6	1.03
12.5	203	143.0	18.9	1.02

[a]Tested at Westinghouse Research Laboratory [10].

Table 4--(Continued).

(b) Center-crack tension specimens.

t, mm	W, mm	a_o, mm	Experimental P_f, kN	$\frac{P_{pred}}{P_{exp}}$
12.6	127	26.2	302	1.06
12.6	127	25.2	311	1.03
12.6	254	51.2	581	1.05
12.6	254	52.1	574	1.06

(c) Three-hole crack specimens.

t, mm	W, mm	a_o, mm	Experimental P_f, kN	$\frac{P_{pred}}{P_{exp}}$
12.6	254	13.9	754	1.05
12.5	254	25.7	738	1.06
12.5	254	38.6	735	1.04
12.5	254	51.8	718	1.04
12.6	254	64.3	696	1.02
12.6	254	75.8	660	1.01
12.5	254	90.0	580	1.04
12.5	254	101.5	505	1.04

Table 5--Stainless steel 304.

(a) Compact specimens.

t, mm	W, mm	a_o, mm	Experimental P_f, kN	$\frac{P_{pred}}{P_{exp}}$
13.1	51	16.5	52.7	0.95
13.3	51	16.3	53.6	0.94
12.8[a]	51	25.6	27.3	0.87
12.8[a]	51	26.1	25.9	0.91
12.8[a]	51	25.8	26.8	0.88
13.1	51	25.8	27.5	0.88
13.1	51	26.2	26.9	0.90
13.2	51	36.2	9.56	0.85
13.1	51	36.2	9.61	0.85
13.4	102	34.1	93.4	1.09
13.3	102	31.1	104.	0.98
13.0[a]	102	49.4	55.1	0.93
13.0[a]	102	50.7	50.8	1.01
13.0[a]	102	51.4	47.8	1.07
13.0	102	50.5	51.8	0.99
13.3	102	51.8	50.6	1.03
13.4	102	72.1	17.7	0.90
13.3	102	72.3	17.3	0.92
13.5	203	62.0	195.	b
13.5	203	62.0	192.	b
12.8[a]	203	102.0	86.8	1.13
12.8[a]	203	102.3	85.4	1.15
12.8[a]	203	102.0	85.3	1.15
13.4	203	101.4	96.3	1.02
13.4	203	102.2	96.1	1.03
13.3	203	142.6	34.1	0.97
13.4	203	142.8	32.9	1.01

[a]Tested at Westinghouse Research Laboratory [10].

[b]Prediction was not made on this specimen.

Table 5--(Continued).

(b) Center-crack tension specimens.

t, mm	W, mm	a_o, mm	Experimental P_f, kN	$\frac{P_{pred}}{P_{exp}}$
13.6	127	26.1	458	1.12
13.6	127	26.2	469	1.09
13.5	254	50.1	882	1.11
13.6	254	50.8	878	1.11

(c) Three-hole crack specimens.

t, mm	W, mm	a_o, mm	Experimental P_f, kN	$\frac{P_{pred}}{P_{exp}}$
13.6	254	13.5	1260	[a]
13.6	254	26.3	1220	a
13.5	254	39.1	1180	a
13.4	254	51.6	1150	a
13.5	254	64.4	1120	a
13.5	254	77.7	999	1.11
13.6	254	89.8	895	1.09
13.6	254	102.7	790	1.08

[a]Prediction was not made on this specimen.

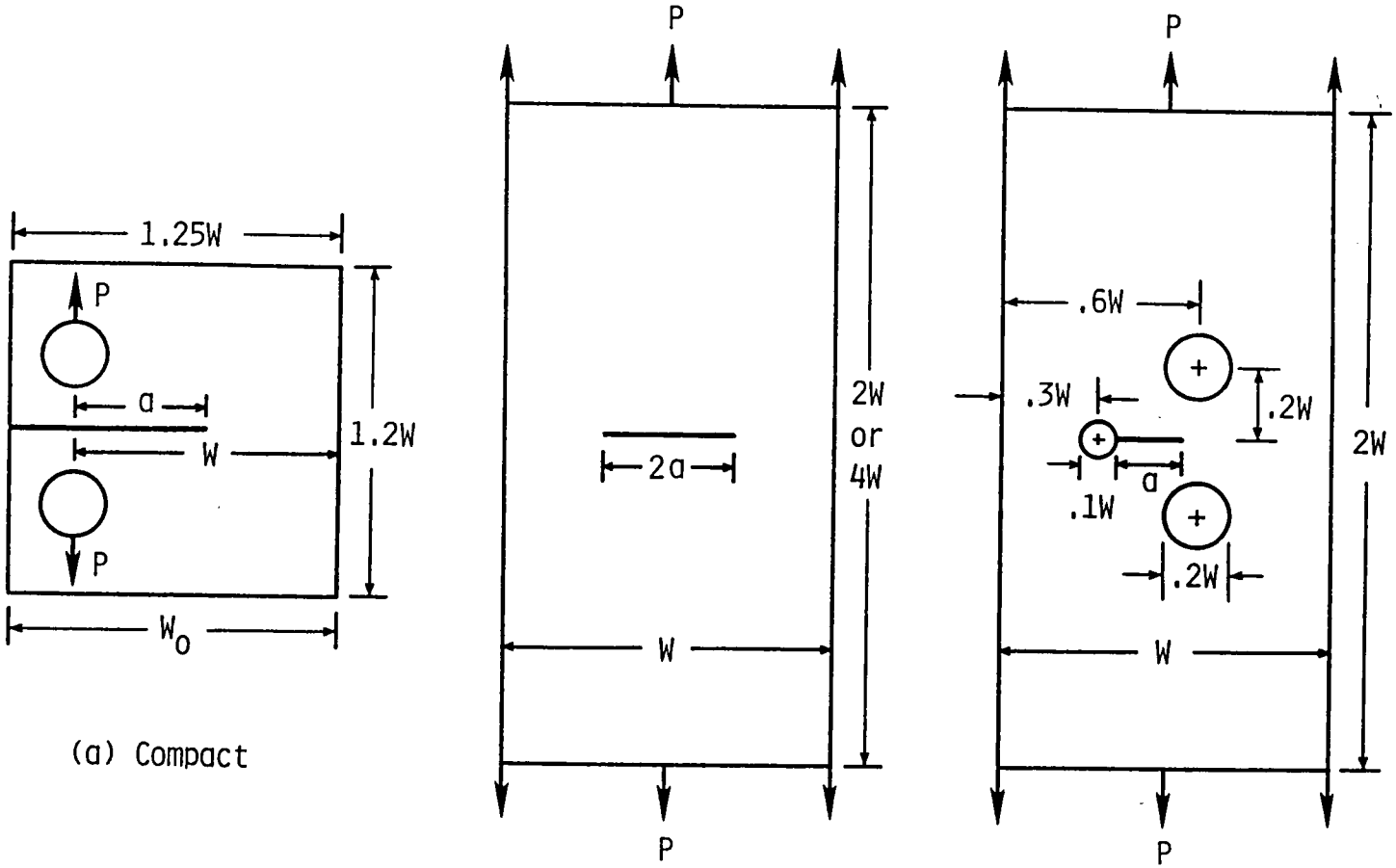

Figure 1.- Specimen configurations tested and analyzed.

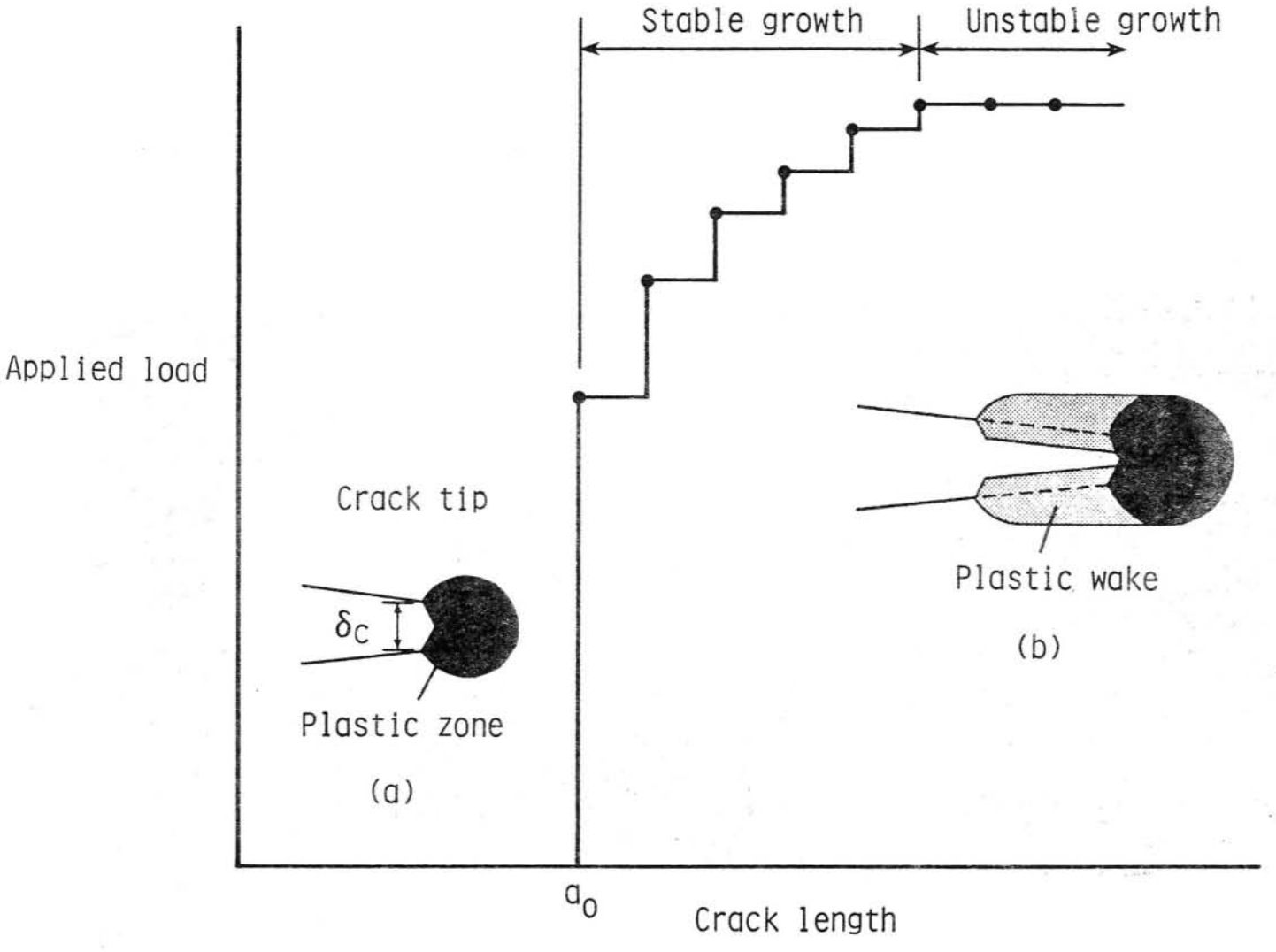

Figure 2.- Typical crack-growth behavior under monotonic loading to failure.

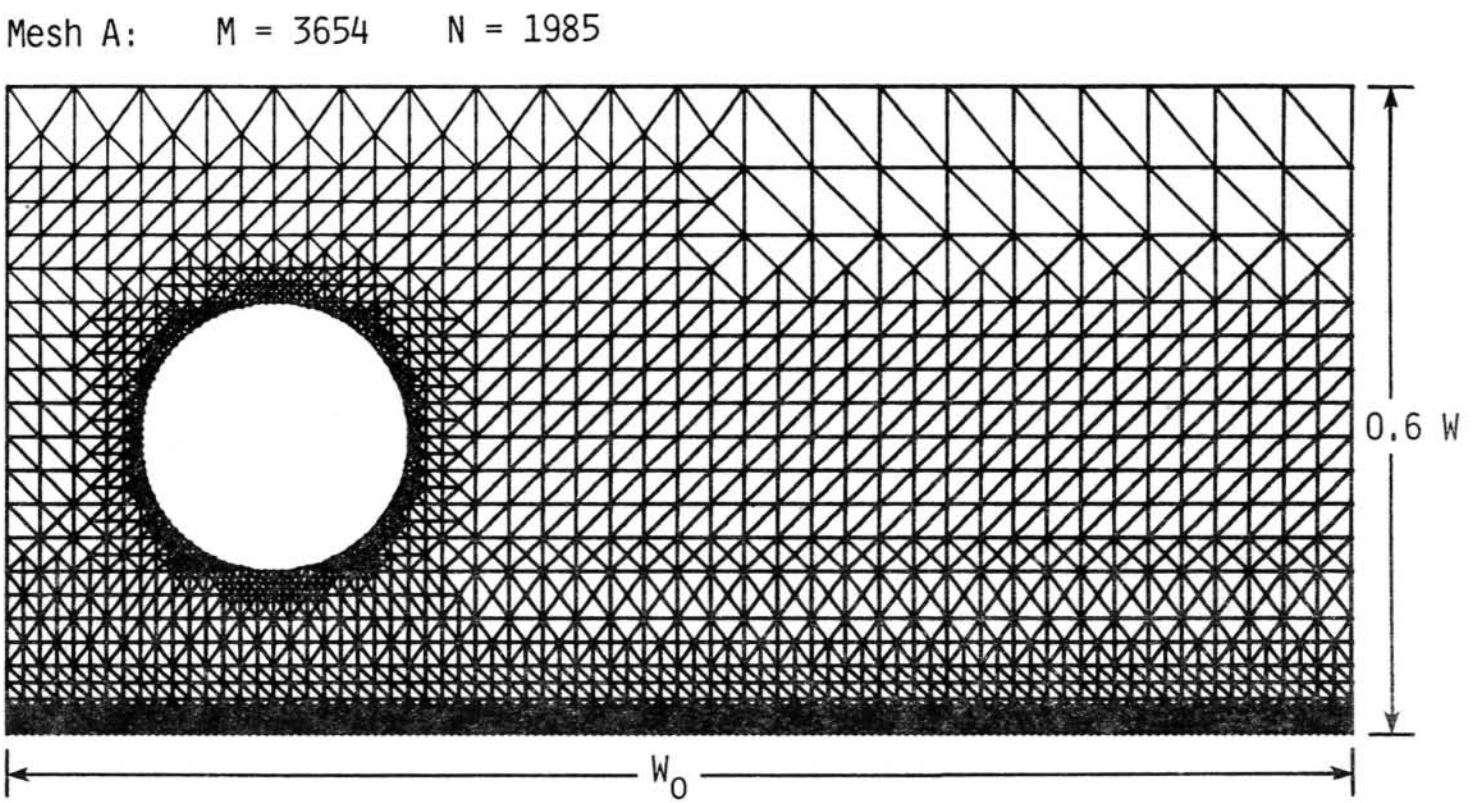

Figure 3.- Finite-element idealization of one-half of the compact specimen.

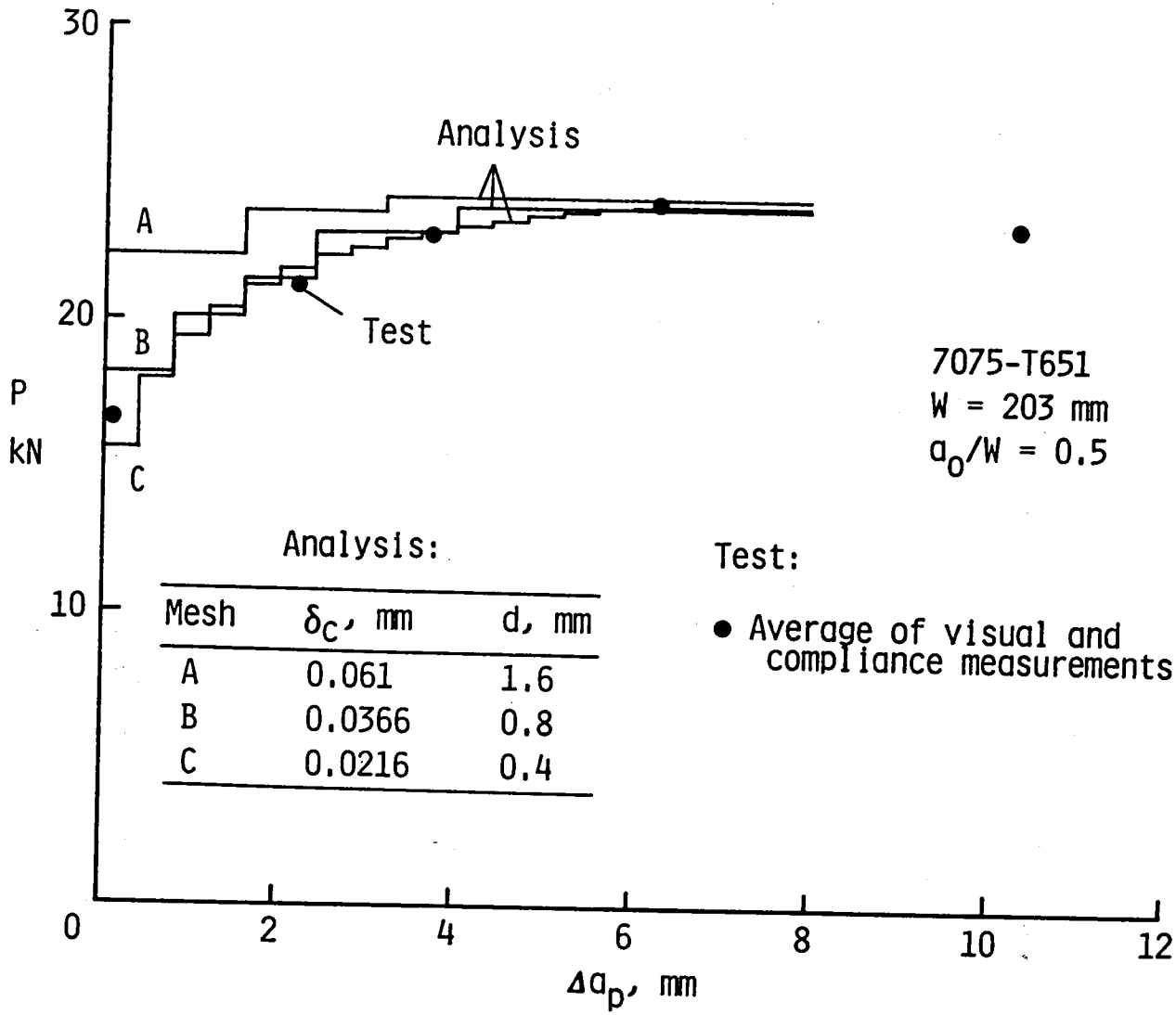

Mesh	δ_c, mm	d, mm
A	0.061	1.6
B	0.0366	0.8
C	0.0216	0.4

Figure 4.- Effect of mesh size and critical CTOD on crack growth.

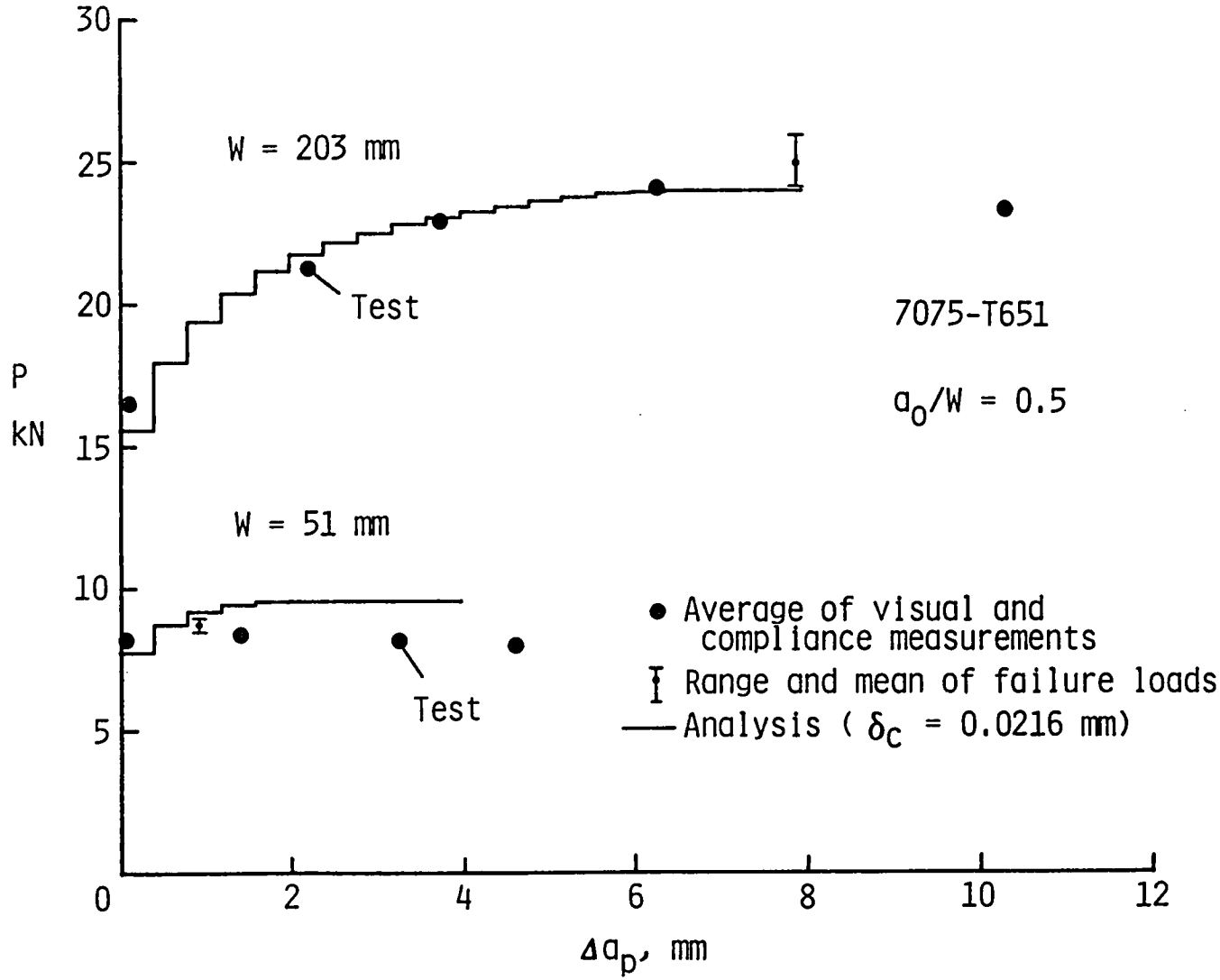

Figure 5.- Comparison of calculated and experimental crack-growth behavior for 7075-T651 aluminum alloy compact specimens.

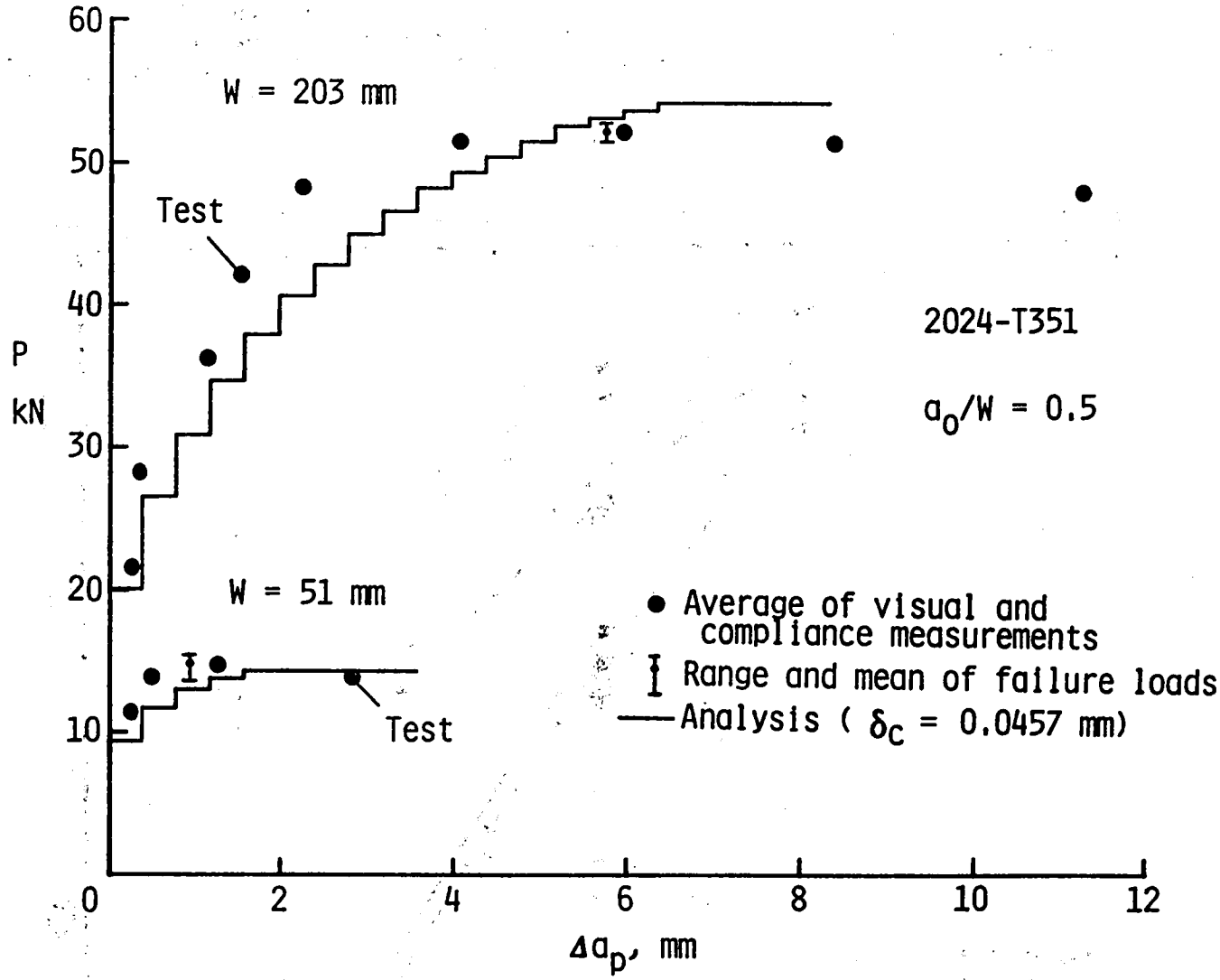

Figure 6.- Comparison of calculated and experimental crack-growth behavior for 2024-T351 aluminum alloy compact specimens.

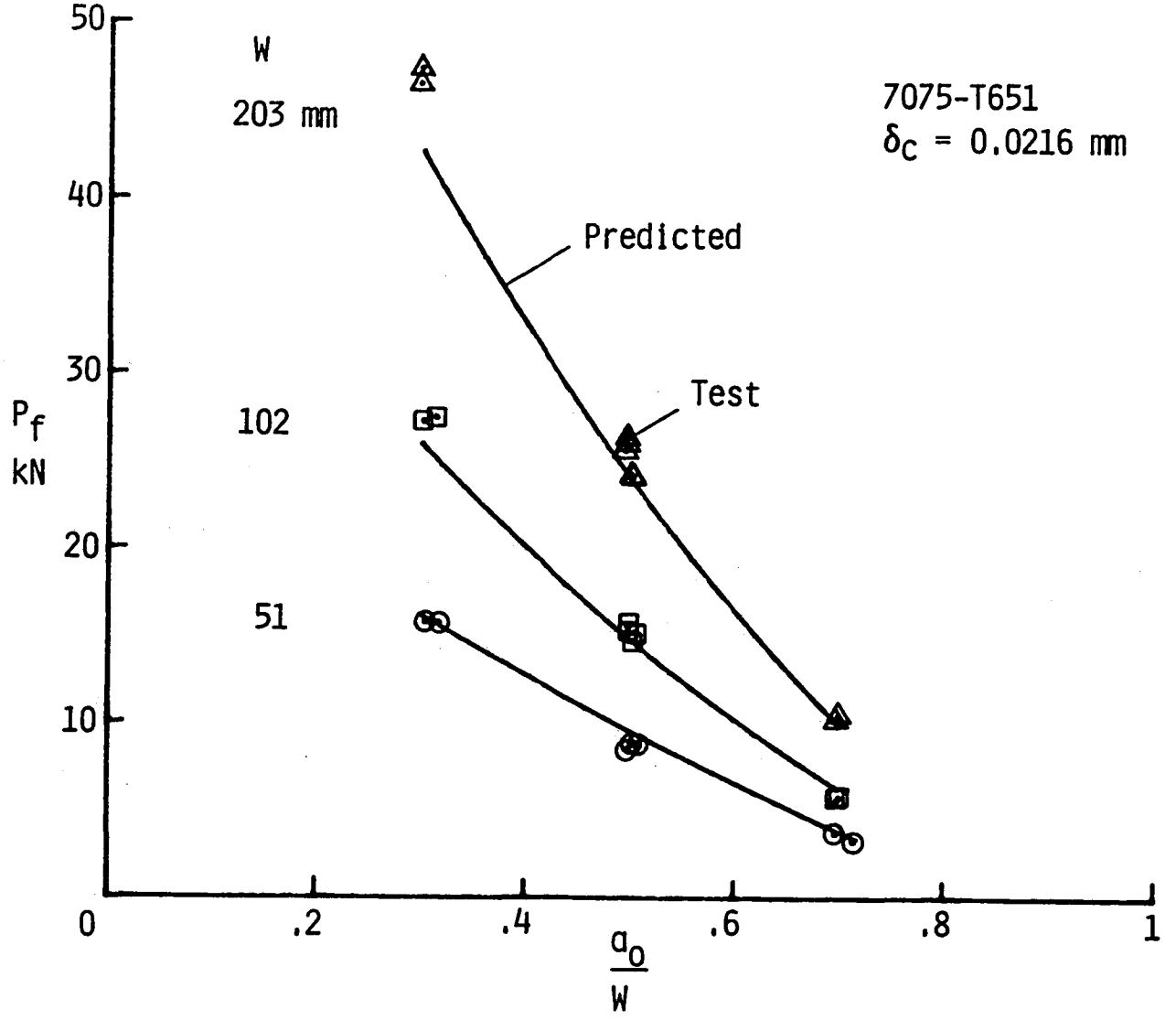

Figure 7.- Comparison of predicted and experimental failure loads for compact specimens made of 7075-T651 aluminum alloy.

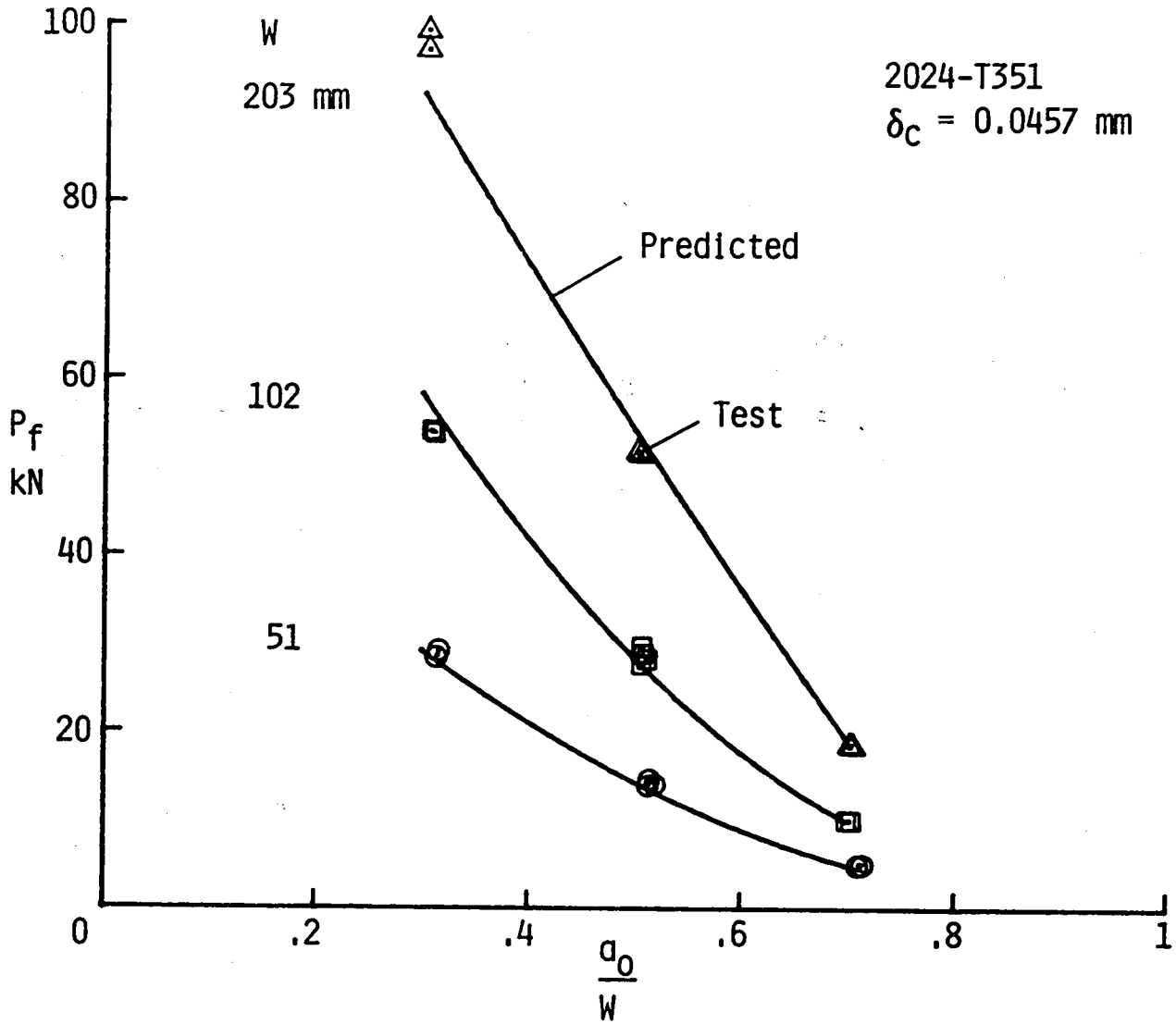

Figure 8.- Comparison of predicted and experimental failure loads for compact specimens made of 2024-T351 aluminum alloy.

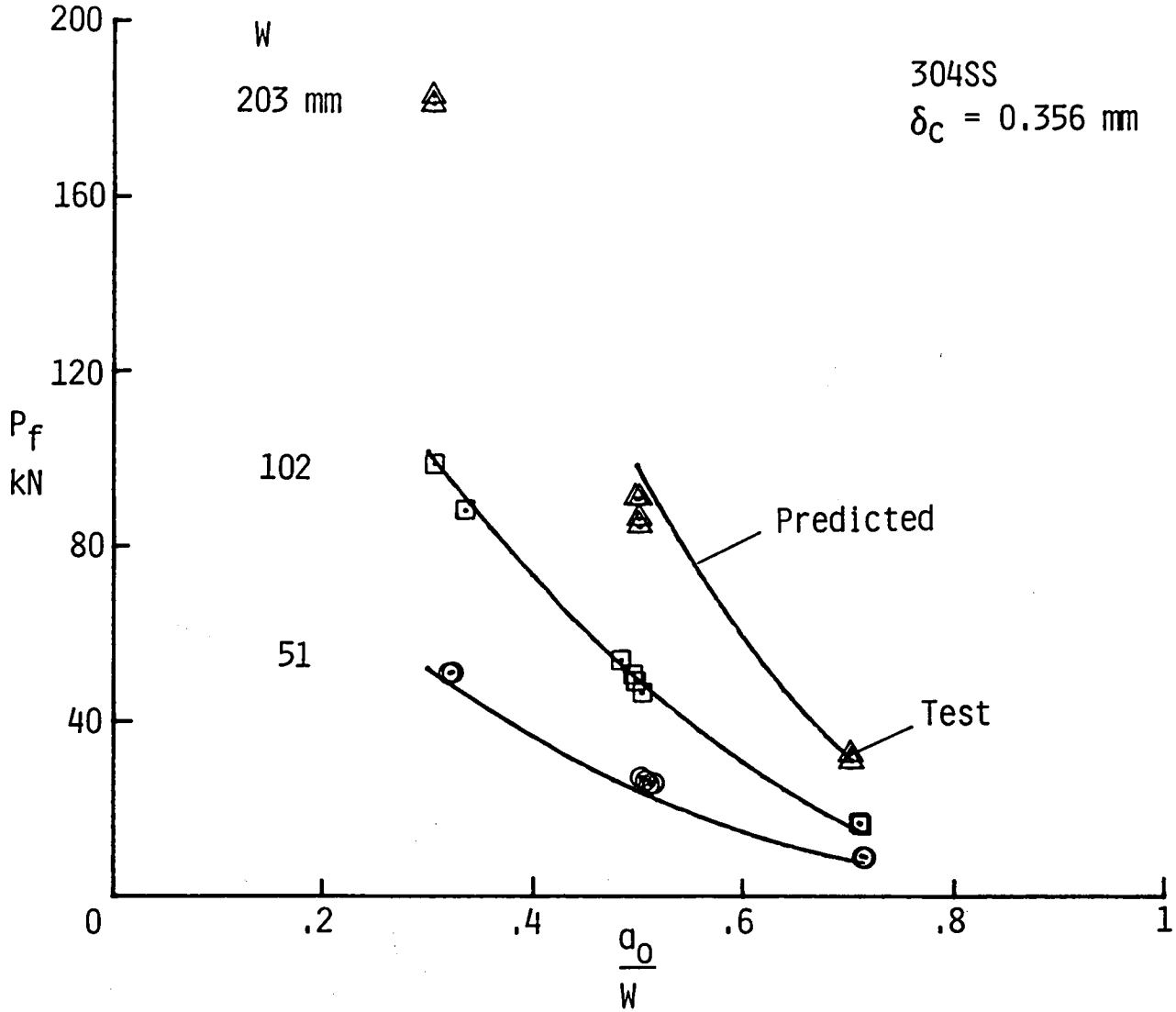

Figure 9.- Comparison of predicted and experimental failure loads for compact specimens made of 304 stainless steel.

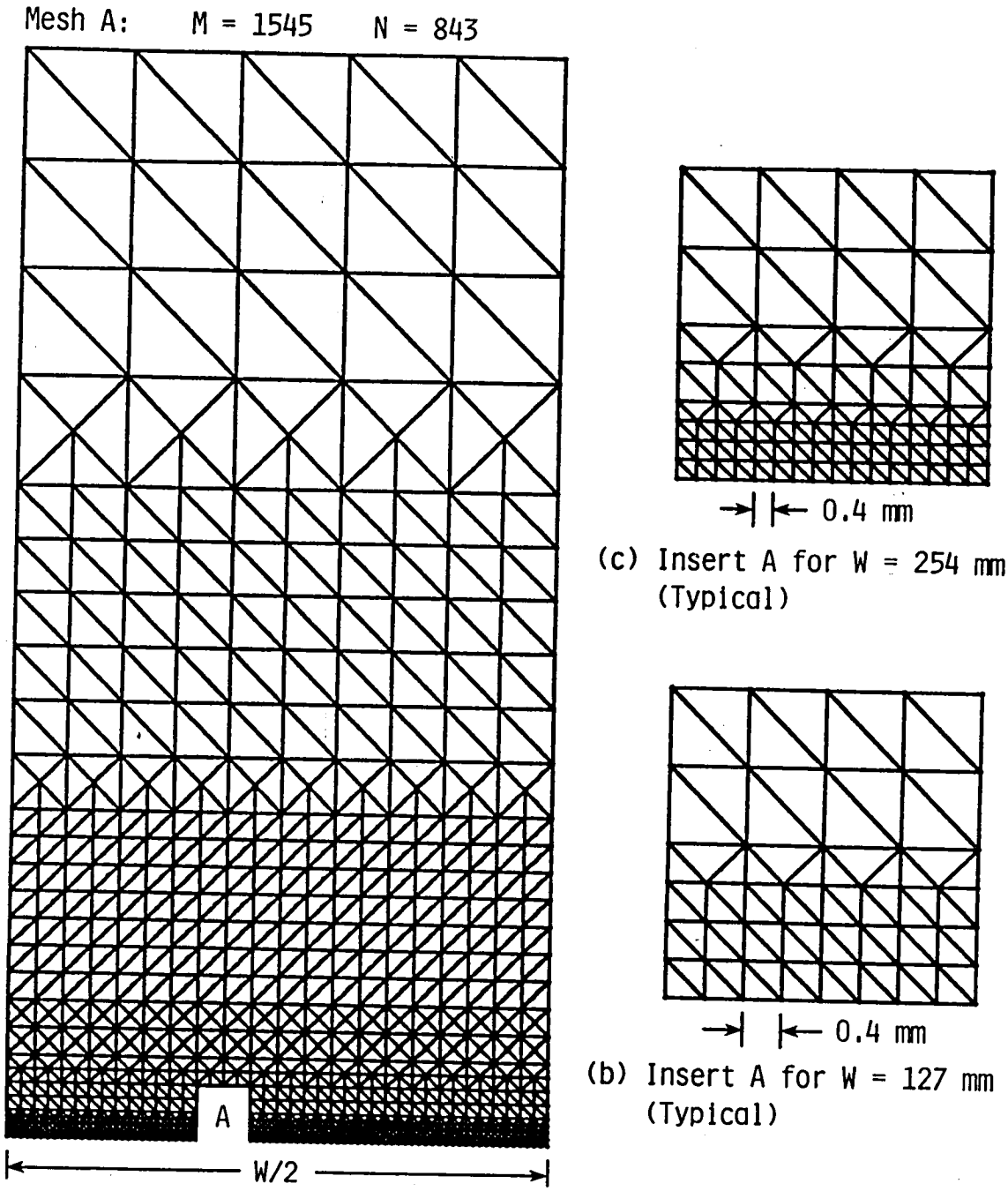

(a) One-quarter of specimen

(c) Insert A for W = 254 mm (Typical)

(b) Insert A for W = 127 mm (Typical)

Figure 10.- Finite-element idealization for center-crack tension specimens.

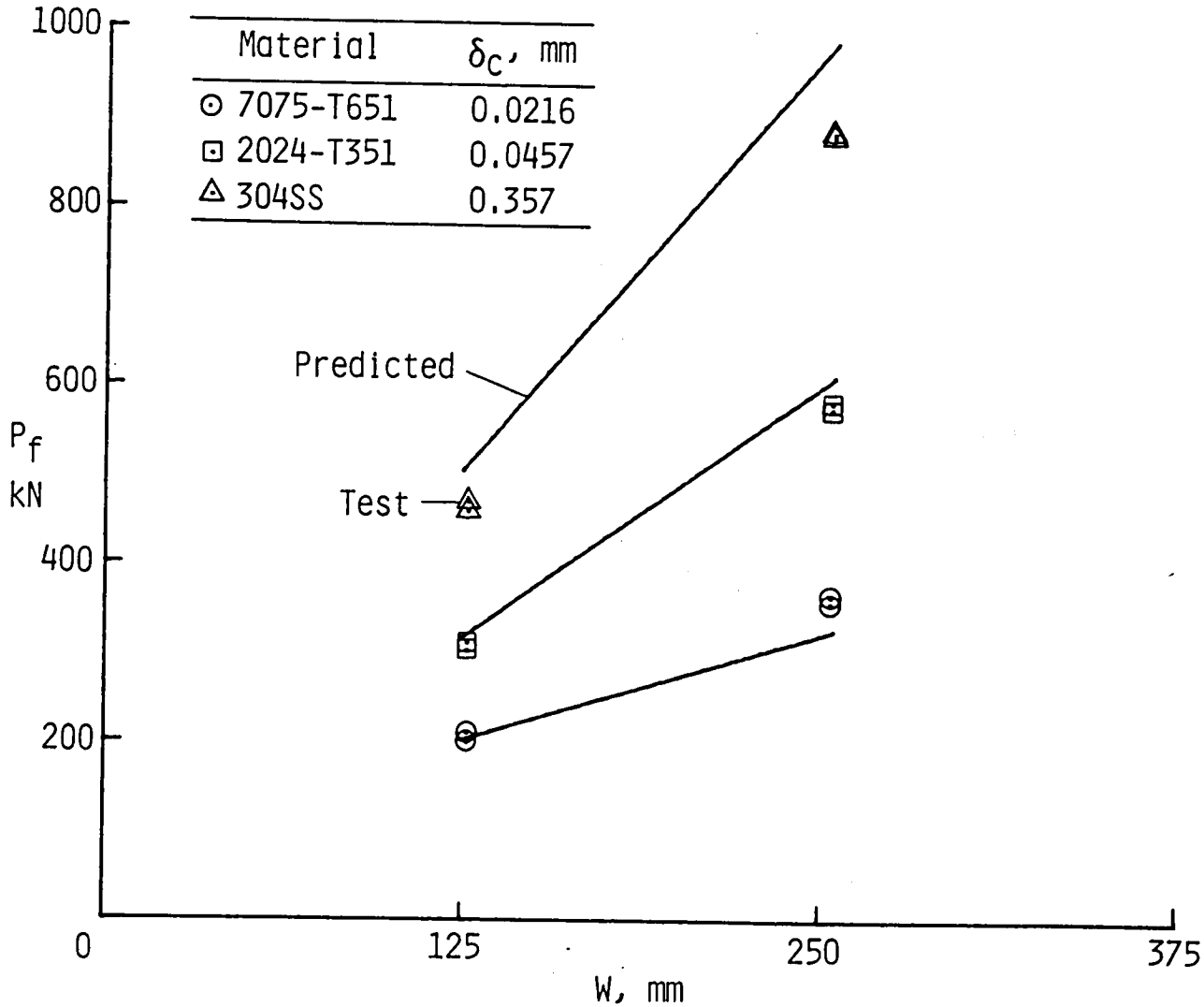

Figure 11.- Comparison of predicted and experimental failure loads for center-crack tension specimens.

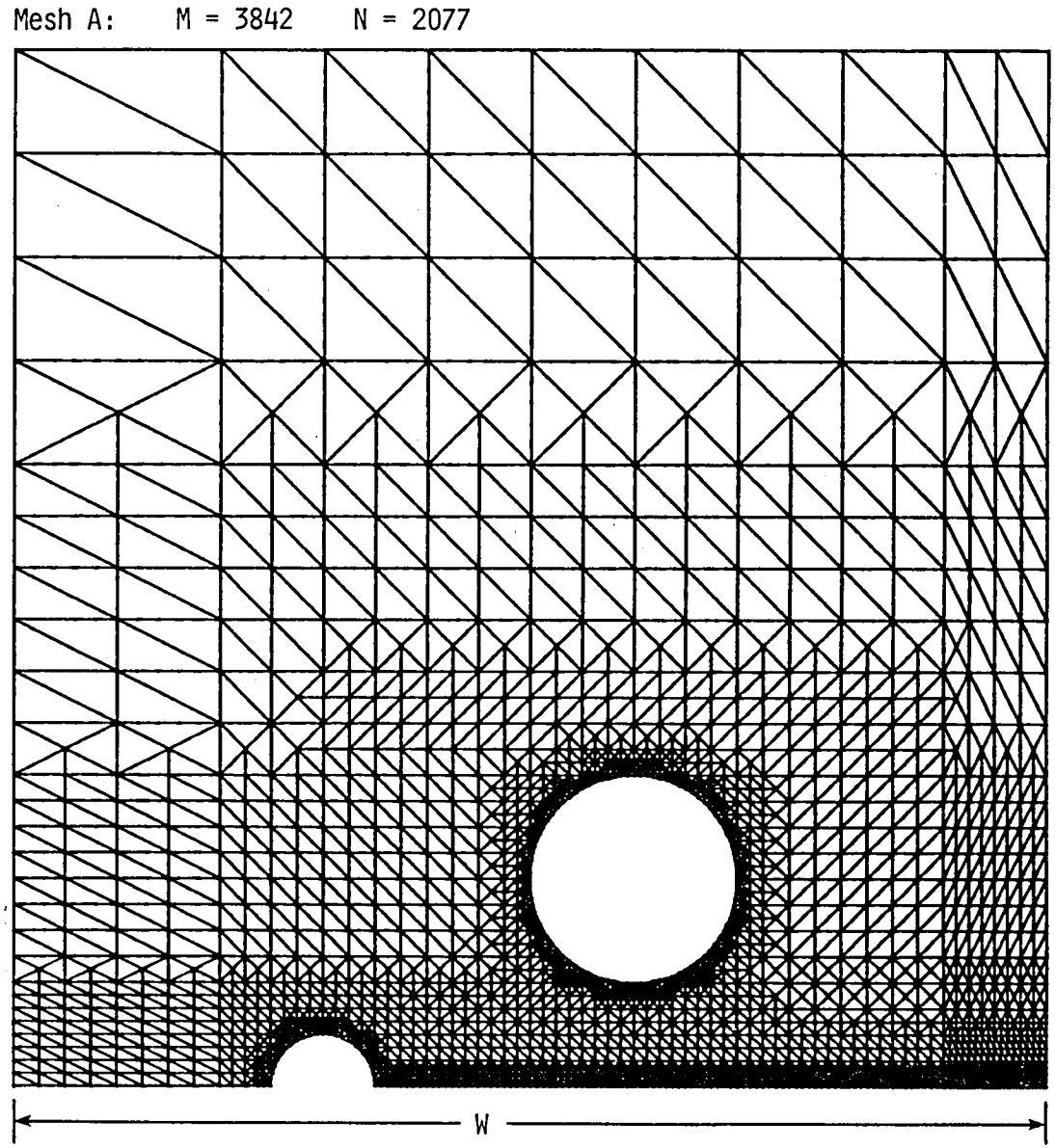

Figure 12.- Finite-element idealization of one-half of the three-hole-crack specimen.

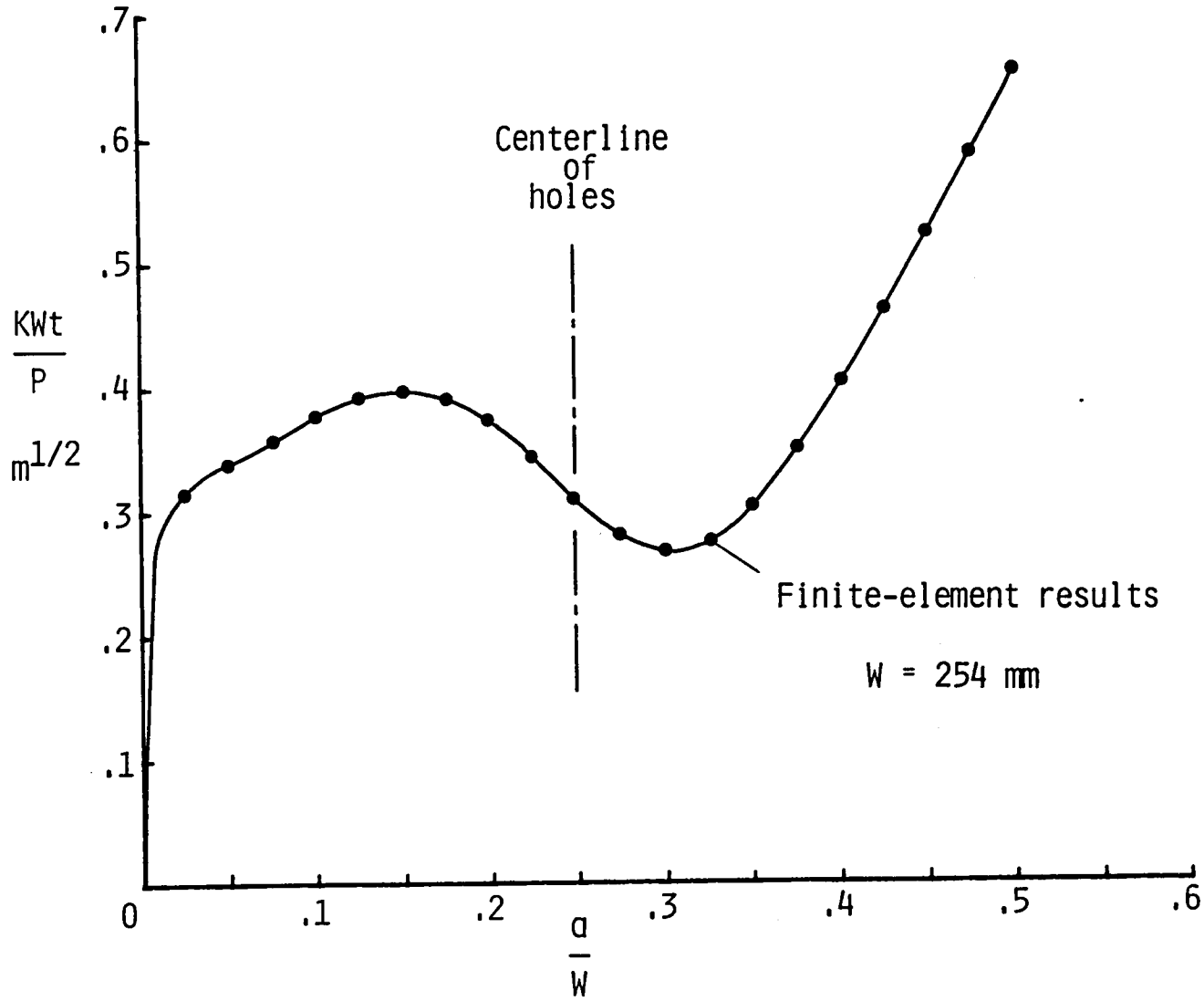

Figure 13.- Stress-intensity factors for the three-hole-crack tension specimen.

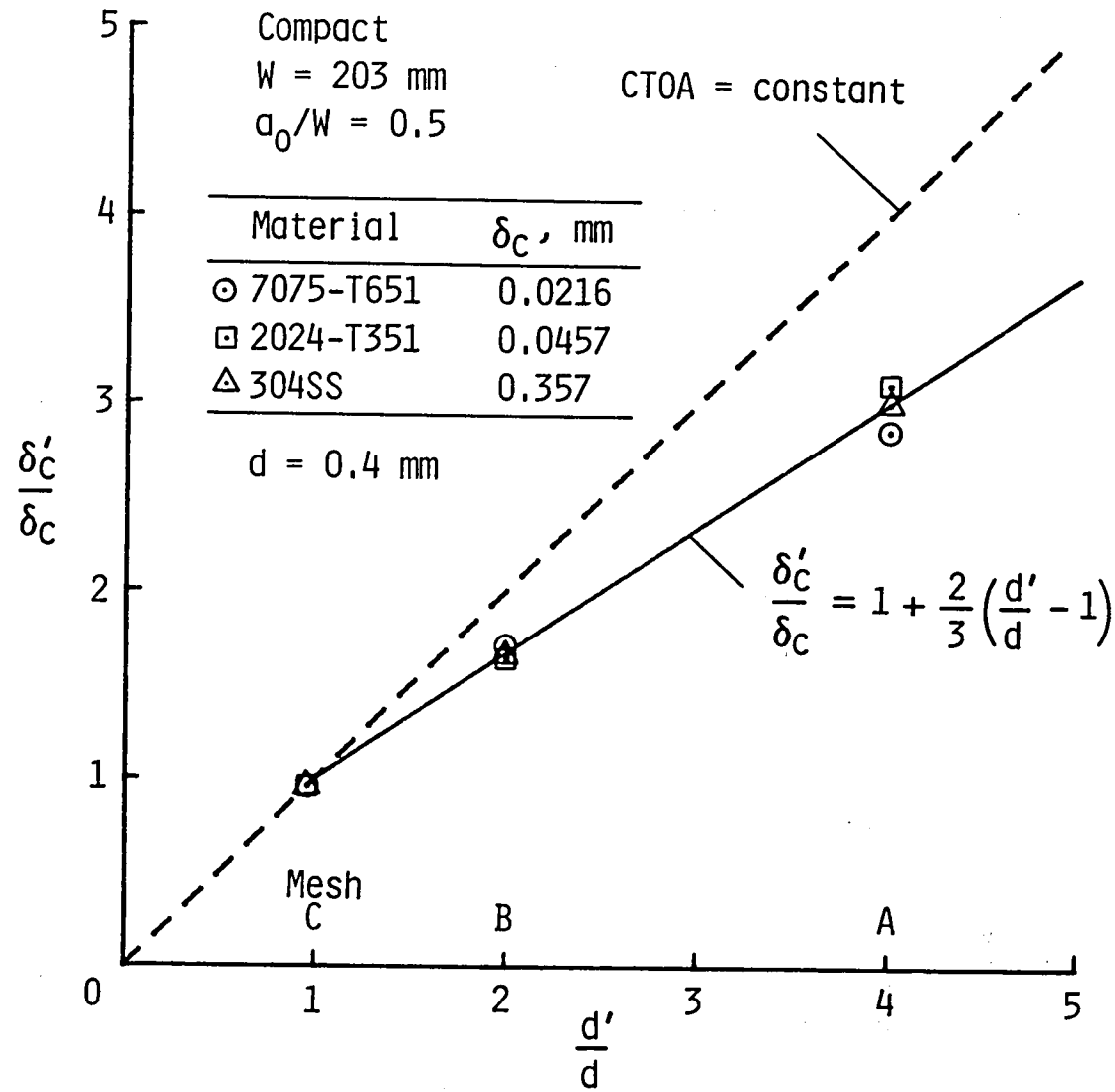

Figure 14.- Effect of mesh size on critical CTOD needed to predict failure loads on the large compact specimens.

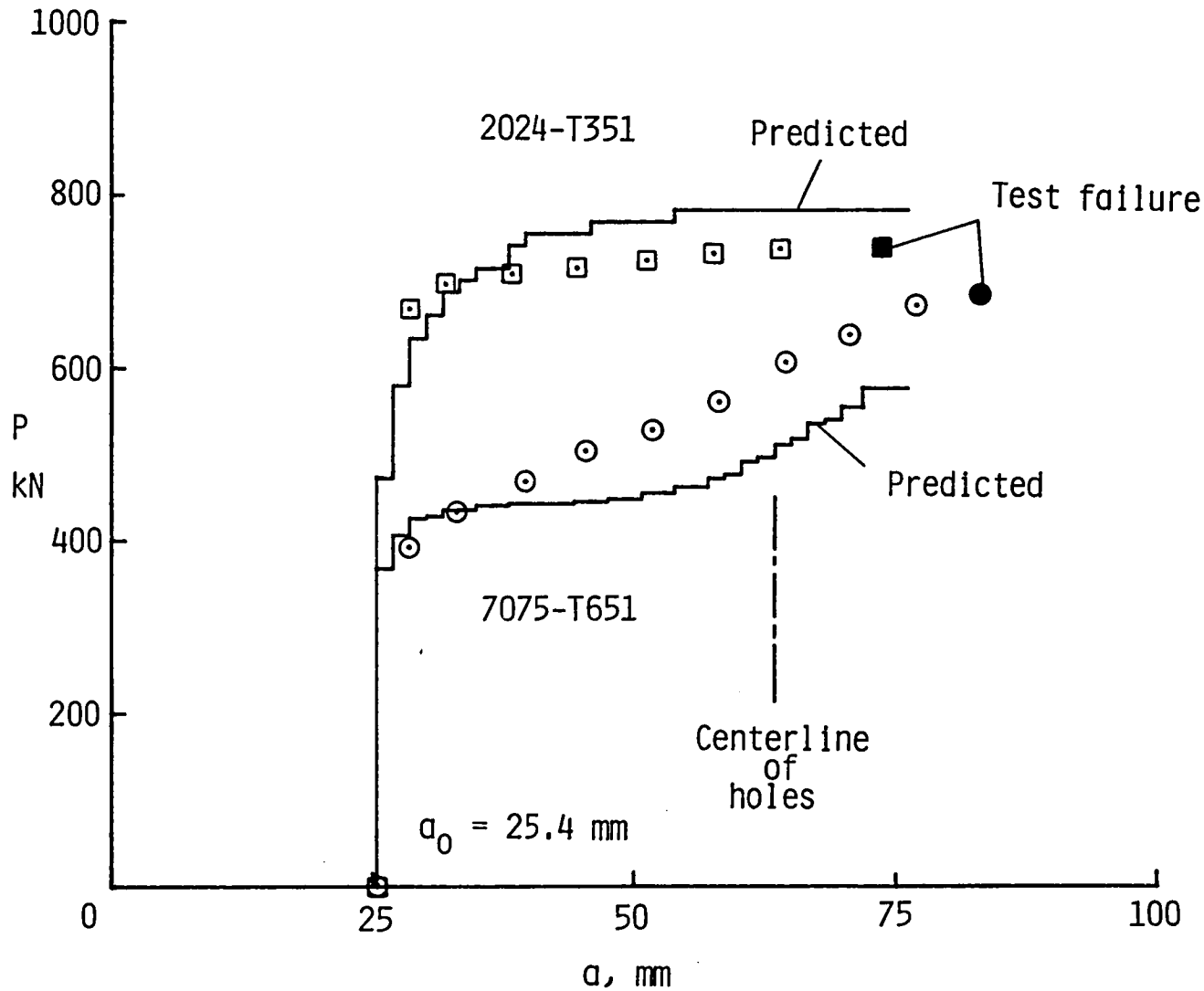

Figure 15.- Comparison of predicted and experimental crack-growth behavior on the three-hole-crack tension specimens.

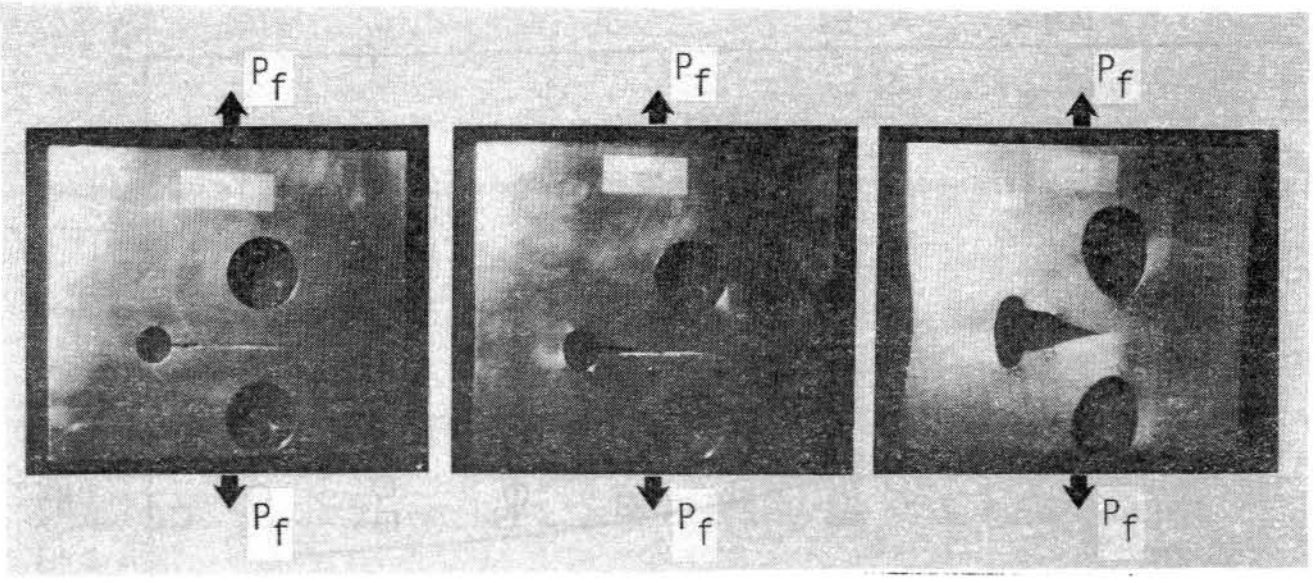

(a) 7075-T651 (b) 2024-T351 (c) 304SS

Figure 16.- Photographs of three-hole-crack tension specimens near maximum load (failure) condition (a_o = 25.4 mm).

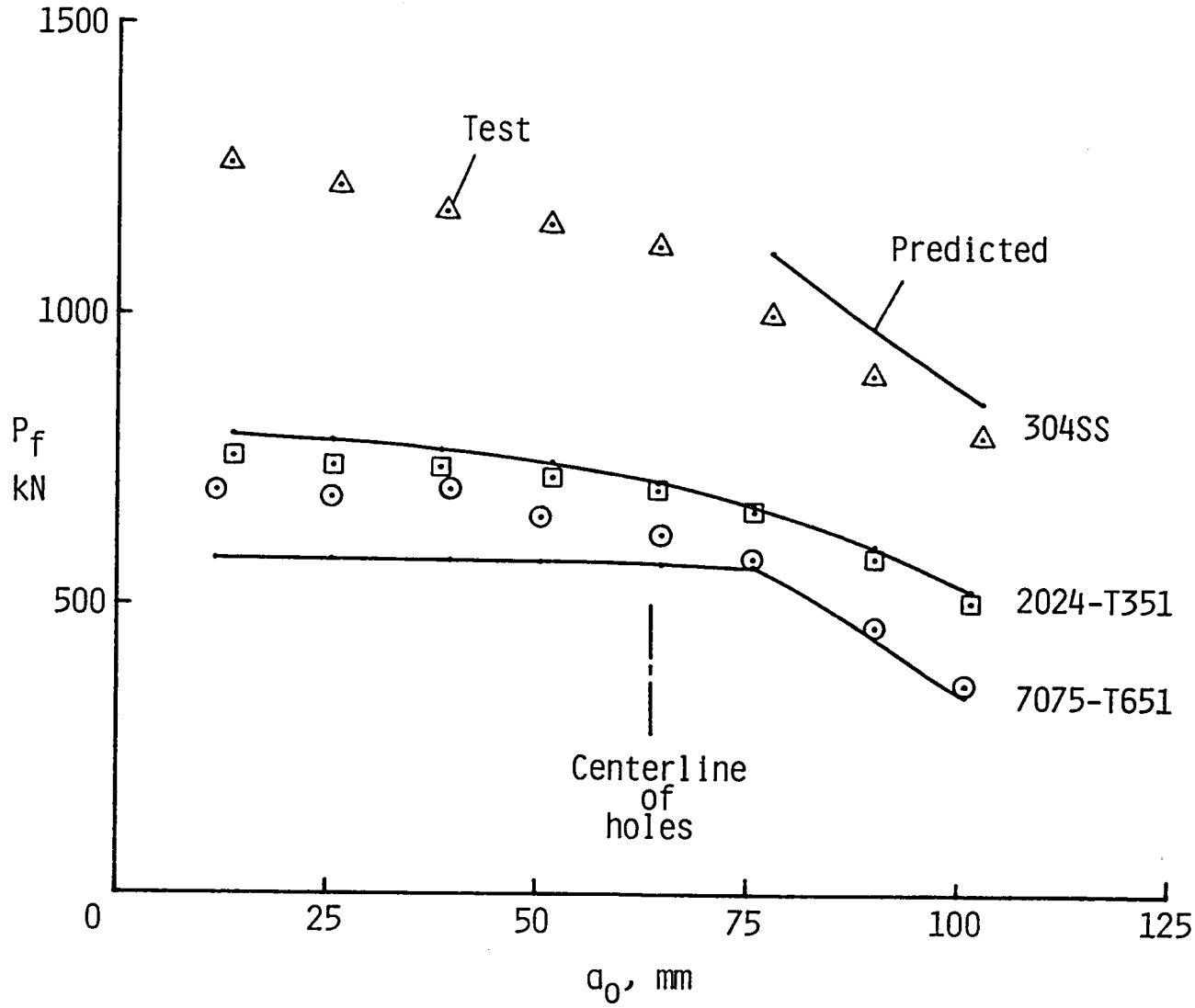

Figure 17.- Comparison of predicted and experimental failure loads on three-hole-crack tension specimens.

1. Report No.	2. Government Accession No.	3. Recipient's Catalog No.
NASA TM-84564		

4. Title and Subtitle	5. Report Date
FINITE-ELEMENT ANALYSIS OF INITIATION, STABLE CRACK GROWTH, AND INSTABILITY USING A CRACK-TIP-OPENING DISPLACEMENT CRITERION	October 1982
	6. Performing Organization Code 505-33-23-02
7. Author(s) J. C. Newman, Jr.	8. Performing Organization Report No.
	10. Work Unit No.
9. Performing Organization Name and Address NASA Langley Research Center Hampton, VA 23665	11. Contract or Grant No.
	13. Type of Report and Period Covered Technical Memorandum
12. Sponsoring Agency Name and Address National Aeronautics and Space Administration Washington, DC 20546	14. Sponsoring Agency Code

15. Supplementary Notes

Presented at the ASTM 15th National Symposium on Fracture Mechanics, College Park, Maryland, July 7-9, 1982.

16. Abstract

An elastic-plastic (incremental and small strain) finite-element analysis was used with a crack-growth criterion to study crack initiation, stable crack growth, and instability under monotonic loading to failure of metallic materials. The crack-growth criterion was a critical crack-tip-opening displacement (CTOD) at a specified distance from the crack tip, or equivalently, a critical crack-tip-opening angle (CTOA). Whenever the CTOD (or CTOA) equaled or exceeded a critical value, the crack was assumed to grow. Single values of critical CTOD were used in the analysis to model crack initiation, stable crack growth, and instability for 7075-T651 and 2024-T351 aluminum alloy compact specimens. Calculated and experimentally measured (from the literature) CTOD values at initiation agreed well for both aluminum alloys. These critical CTOD values from compact specimens were also used to predict failure loads on center-crack tension specimens and a specially-designed three-hole-crack tension specimen made of the two aluminum alloys and of 304 stainless steel. All specimens were 12.7 mm thick. Predicted failure loads for 7075-T651 aluminum alloy and 304 stainless steel specimens were generally within ±15 percent of experimental failure loads, whereas the predicted failure loads for 2024-T351 aluminum alloy specimens were generally within ±5 percent of the experimental loads. The technique presented here can be used as an engineering tool to predict crack initiation, stable crack growth, and instability for cracked structural components from laboratory specimens, such as the compact specimen.

17. Key Words (Suggested by Author(s))	18. Distribution Statement
Instability Crack initiation Stable crack growth Finite-element analysis Elastic-plastic fracture Crack-tip-opening displacement Cracks Aluminums Steels	Unclassified - Unlimited Subject Category 39

19. Security Classif. (of this report)	20. Security Classif. (of this page)	21. No. of Pages	22. Price*
Unclassified	Unclassified	55	A04

* For sale by the National Technical Information Service, Springfield, Virginia 22161